ACS MATERIALS LETTERS

www.acsmaterialsletters.org

A Layered Hydrogen-Bonded Organic Framework with C_3H_6-Preferred Pores for Efficient One-Step Purification of Methanol-to-Olefins (MTO) Products

Yunzhe Zhou, Cheng Chen, Zhenyu Ji, Rajamani Krishna, Zhengyi Di, Daqiang Yuan, and Mingyan Wu*

Cite This: ACS Materials Lett. 2024, 6, 1388–1395

Read Online

ACCESS | Metrics & More | Article Recommendations | Supporting Information

ABSTRACT: Separation of methanol-to-olefins (MTO) products to obtain high-purity C_2H_4 and C_3H_6 is of great importance, since it provides an alternative process for such important industrial raw materials. However, developing adsorbents with high C_2H_4/C_3H_6 selectivity and productivity remains challenging. Herein, we report an ultrastable layered hydrogen-bonded framework (HOF-NBDA), which features C_3H_6 preferred pore with multiple interlaminar interactions with C_3H_6. It delivers an ultrahigh C_3H_6 uptake (3.6 mmol g^{-1}) at 10 kPa, while absorbs only 0.3 mmol g^{-1} C_2H_4 and shows a high C_2H_4/C_3H_6 selectivity (11.1). Experimental breakthroughs show that HOF-NBDA can efficiently separate C_3H_6/C_2H_4 (50/50, v/v) at different flow rates, temperatures, as well as relative humidities and provides a high C_2H_4 productivity (5.7 mol kg^{-1}, purity ≥99.95%). Meanwhile, 4.5 mol kg^{-1} C_3H_6 (purity ≥99.5%) can also be collected during the desorption process. Additionally, thanks to ultrahigh stability, good scalability, and easy regeneration, HOF-NBDA is considered as a promising material for one-step energy-efficient separation of MTO products.

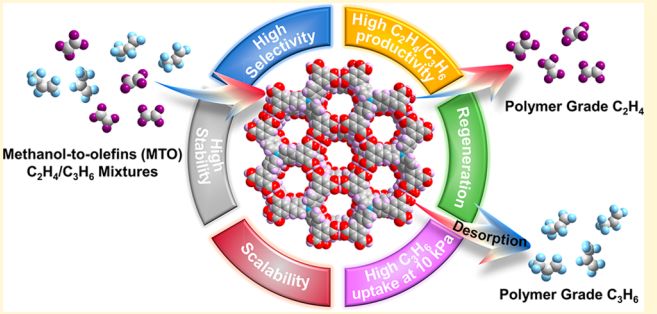

As the most important fundamental raw materials in the petrochemical industry worldwide, ethylene (C_2H_4) and propylene (C_3H_6) have been widely applied to manufacture various chemicals.[1−3] For instance, C_2H_4 is an essential feedstock for the production of polyethylene, synthetic rubber, and other organic chemical products.[4] At the same time, C_3H_6 has been widely used in the field of polypropylene, propylene oxide, and acrylonitrile.[5] With the vigorous development of the chemical manufacturing industry, the global annual production of C_2H_4 and C_3H_6 has exceeded 200 million tons and maintains an annual growth trend.[6−9] However, with the shortage of petroleum resources on which low-carbon olefins production depends, the methanol-to-olefin (MTO) process, an emerging sustainable method for low-carbon olefin preparation, has been considered as an effective compensation for the urgent demand for low olefins. The MTO reaction is an advanced method for preparing C_2H_4 from coal and natural gas, where the products contain ∼21 wt % C_3H_6 and ∼51 wt % C_2H_4.[10−15] Therefore, the purification of MTO products to obtain high-purity C_3H_6 and C_2H_4 is essential for downstream applications and the sustainability of the chemical manufacturing industry. The common separation process of C_3H_6 and C_2H_4 mixtures mainly depends upon cryogenic distillation at high pressure, requiring large energy consumption that does not match the requirements of green chemistry.

Adsorptive separation sensibly has been deemed as an energy-efficient and practical technology, considering that the conventional separation processes of cryogenic distillation and alkaline washing are highly energy- and capital-intensive. In this case, the use of porous materials for adsorption separation is proposed as a prospective alternative method. Adsorption separation is more energy efficient than traditional techniques, but is closely dependent on adsorbents that require high adsorption capacity and selectivity for gas mixtures.[16] Over the past two decades, numerous types of porous sorbents, such as

Received: January 12, 2024
Revised: March 4, 2024
Accepted: March 4, 2024

https://doi.org/10.1021/acsmaterialslett.4c00111
ACS Materials Lett. 2024, 6, 1388−1395

conventional activated carbons and zeolites, as well as emerging metal−organic frameworks (MOFs) and covalent organic frameworks (COFs), have been widely investigated as new promising adsorbents for the separation of light hydrocarbons mixtures, such as C_2H_6/C_2H_4, C_3H_8/C_3H_6, C_2H_2/CO_2, C_2H_2/C_2H_4, and so on.[17−23] Unlike other gas separation systems such as C_2H_4/C_2H_6 and C_3H_6/C_3H_8, which have different functional groups, both C_2H_4 and C_3H_6 have the same unsaturated C═C chemical bonds, and the physical and chemical properties are much more similar. Consequently, some porous materials with open metal sites which can be weakly coordinated by C═C chemical bonds or electronegative functional groups which can interact with positively charged H atoms in olefins, will meanwhile increase the interactions with C_2H_4 and C_3H_6, which are not conducive to separating the two components.[24−26] More recently, although several adsorbents have been constructed for C_2H_4/C_3H_6 separation, the comparatively low C_2H_4/C_3H_6 selectivity and productivity motivate the development of high-efficiency C_2H_4/C_3H_6 separation materials. Closer inspection of the C_3H_6 and C_2H_4 molecules reveals a subtle difference: the C_3H_6 molecule possesses an extra sp^3 hybrid carbon atom, which not only enlarges the molecule size of C_3H_6, but also provides more C−H bonds than C_2H_4, but also increases its polarizability (polarizability of C_3H_6 = 62.6 × 10^{-25} cm^3; polarizability of C_2H_4 = 42.52 × 10^{-25} cm^3). Therefore, constructing porous materials by pure organic aromatic ligands with nonpolar surfaces, which can provide more C−H···π interactions, is beneficial for trapping C_3H_6 molecules.[27]

Hydrogen-bonded organic frameworks (HOFs), which represent a kind of emerging porous material which is generally self-assembled by conjugated organic units through intermolecular hydrogen-bonding interactions, usually possess nonpolar channels and have been proven to be greatly beneficial for trapping gas molecules with higher polarizability.[28−31] For example, HOF-76a,[32] reported by Chen and Li et al., can prefer absorbing ethane (C_2H_6) over C_2H_4 and realize the one-step purification of C_2H_4 from the C_2H_4/C_2H_6 mixture. Consequently, it is speculated that HOFs may also exhibit excellent potential in capturing C_3H_6 from C_2H_4/C_3H_6 mixtures. At the same time, consecutive π···π interactions are always employed to stabilize the frameworks of HOFs in the self-assembly progress,[33−36] which may result in a two-dimensional (2D) layered structure. Therefore, more supramolecular interaction sites for large gas molecules such as C_3H_6 can be available across these different layers, which is conducive to the efficient separation of C_2H_4/C_3H_6.[37,38] Additionally, for actual industrial applications, a desired adsorbent should not only have optimal balance between adsorption capacity and selectivity, but also have excellent performance in stability, regeneration, and easy scalability of synthesis.[39−41] And then, since HOFs aggregate together through the supramolecular interactions, they can be regenerated by simple recrystallization on a large scale.[42−45] Thus, designing HOFs with layered structure and a specific pore environment could not only realize efficient C_2H_4/C_3H_6 separation but also be meaningful to achieve practical application in rigorous industrial environments.

Based on the above considerations, we herein report a layered hydrogen-bonded organic framework HOF-NBDA, which is created by an organic ligand for a planar hexacarboxylic acid and possesses a two-dimensional (2D) structure with a particular −ABCD− stacking model. Benefiting from the particularity of its structure and nonpolar pore surface, HOF-NBDA exhibits a large difference between the affinity of C_3H_6 and that of C_2H_4. At 298 K and 1 bar, HOF-NBDA shows a high uptake of C_3H_6 (5.3 mmol g^{-1}), while the absorption capacity of C_2H_4 is relatively low (2.9 mmol g^{-1}). More importantly, the uptake of C_3H_6 at 10 kPa can reach 3.6 mmol g^{-1}, while the uptake of C_2H_4 is only 0.3 mmol g^{-1}. The uptake ratio is 10.5, surpassing all reported porous materials. Due to the significant difference in C_3H_6 and C_2H_4 uptakes, HOF-NBDA performs well in separating C_2H_4/C_3H_6 (50/50, v/v). After one circle of the separation and desorption experiment under ambient conditions, 5.7 mol kg^{-1} of high-purity (≥99.95%) C_2H_4 and 4.5 mol kg^{-1} of C_3H_6 with a purity of ≥99.5% could be obtained. In addition, HOF-NBDA can retain excellent C_2H_4/C_3H_6 separation performance under different gas flow rates, temperatures, and relative humidity conditions, which is rarely seen in gas separation materials. Furthermore, theoretical calculations reveal that the 2D structure and nonpolar surfaces of HOF-NBDA supply many more supramolecular interactions with C_3H_6 than C_2H_4, which play a crucial role in their remarkable C_2H_4/C_3H_6 separation performance. This nonpolar pore environment strategy provides a new way to design porous materials with excellent C_2H_4/C_3H_6 separation performance.

HOF-NBDA can be obtained as yellow crystals by a simple solution diffusion method. As shown in Figure 1a, six carboxylic acid groups in the H_6NBDA molecule exist in one plane and connect with three adjacent H_6NBDA through carboxylic acid dimers to form a honeycomb net with two types of hexagonal windows (Figure 1b). Then, 2D hexagonal sheets in HOF-NBDA are arranged in a particular −ABCD− manner through interlaminar $\pi-\pi$ interactions, resulting in a 1D channel with a moderate size of ca. 8.4 Å (calculated by a *zeo++* package) along the *a*-axis (Figures 1c and 1d). For the

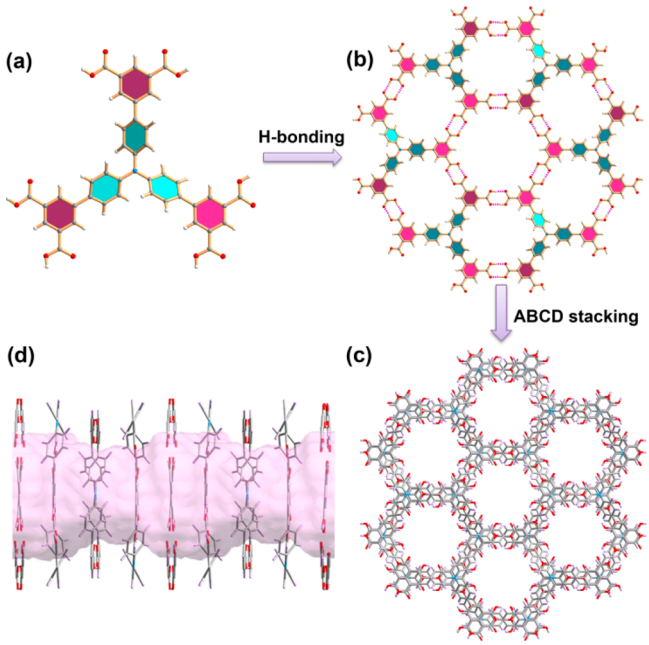

Figure 1. (a) The molecular structure of H_6NBDA. (b) Representation of the two kinds of hexagonal windows and the resulting monolayer network in HOF-NBDA. (c) The layered frameworks are stacked in slippage in an −ABCD− manner without interpenetration. (d) 1D channel in the framework.

https://doi.org/10.1021/acsmaterialslett.4c00111
ACS Materials Lett. 2024, 6, 1388−1395

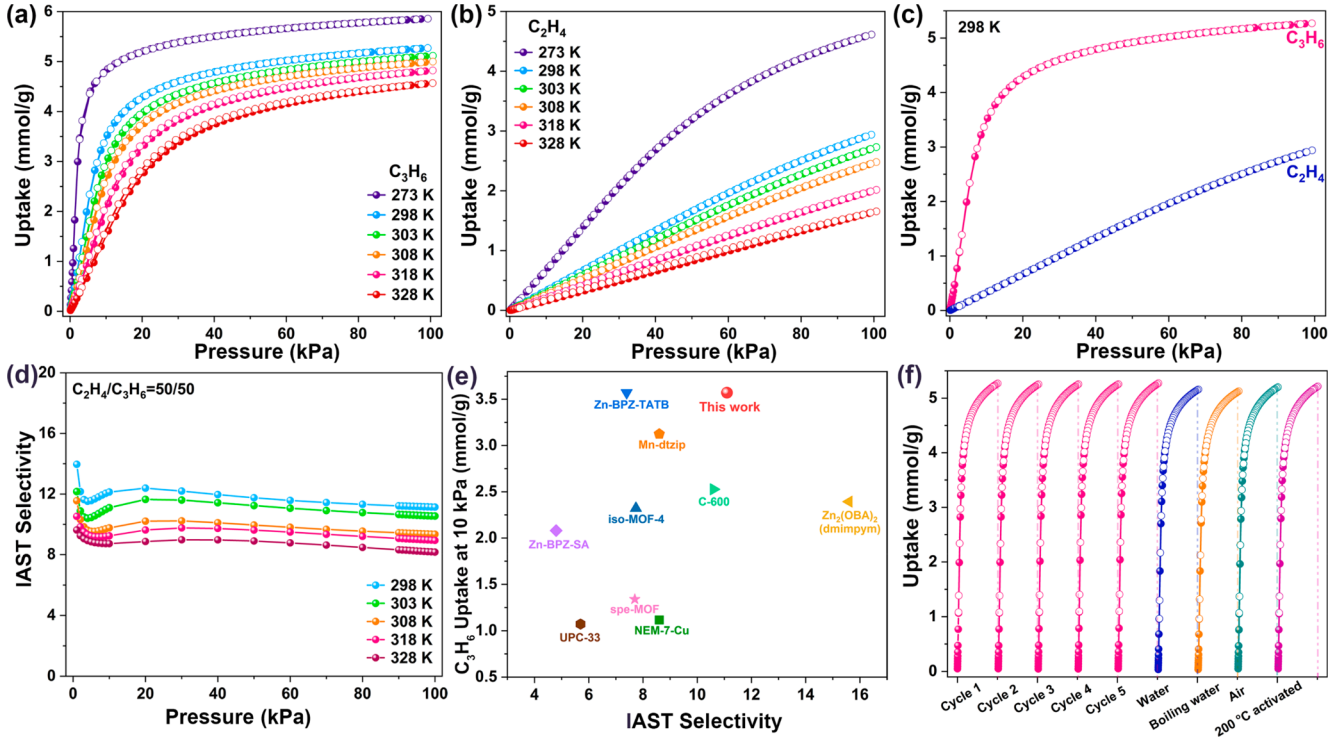

Figure 2. (a, b) Single-component adsorption isotherms of C_3H_6 and C_2H_4 at 273−328 K. (c) Comparison of adsorption isotherms of C_3H_6 and C_2H_4 at 298 K. (d) IAST selectivity of HOF-NBDA for 50/50 C_2H_4/C_3H_6 at 298, 303, 308, 318, and 328 K, respectively. (e) Comparison of C_2H_4/C_3H_6 selectivity and the C_3H_6 uptake at 10 kPa for HOF-NBDA and top-performing C_3H_6-selective materials. (f) Five cycles of C_3H_6 adsorption at 298 K and C_3H_6 adsorption isotherms after different treatments for HOF-NBDA at 298 K.

HOFs with a planar honeycomb net, the hexagonal layers generally stack in the AA mode and interpenetrate with each other,[46−51] which is entirely different from HOF-NBDA. Furthermore, the unique stacking model results in the staggered arrangement of carboxylic acid dimers and benzene rings in adjacent layers in HOF-NBDA, which may provide more synergistic supramolecular interaction sites for gas molecules with more C−H groups.

Motivated by the particular layer structure and special pore environment of HOF-NBDA, we have conducted single-component adsorption isotherms for C_3H_6 and C_2H_4 in the range of 273−328 K. As shown in Figures 2a and 2b, HOF-NBDA manifests steep and high uptakes of C_3H_6, while the adsorption isotherms of C_2H_4 are relatively flat at the same temperature. At 298 K, when the pressure rises to 1 bar, the uptake of C_3H_6 reaches 5.3 mmol g^{-1} (Figure 2c), which is considerably higher than well-known porous materials with top performance of C_2H_4/C_3H_6 separation, including $Zn_2(oba)_2(dmimpym)$ (3.4 mmol g^{-1}),[52] UPC-33 (4.2 mmol g^{-1}),[53] and NEM-7-Cu (3.4 mmol g^{-1}).[54] Under the same conditions, the C_2H_4 uptake is only 2.9 mmol g^{-1}. Furthermore, the adsorption isotherms of C_3H_6 increased more sharply than that of C_2H_4, especially in the low-pressure region. At 10 kPa, the adsorption capacity of C_3H_6 at 298 K can reach 3.6 mmol g^{-1}, surpassing almost all reported outstanding materials for C_2H_4/C_3H_6 separation (see Figure 2e, as well as Table S1), such as Zn-BPZ-SA (2.1 mmol g^{-1}),[25] iso-MOF-4 (2.2 mmol g^{-1}),[55] spe-MOF (1.3 mmol g^{-1}),[26] NEM-7-Cu (1.1 mmol g^{-1}),[54] and Mn-dtzip (3.1 mmol g^{-1}).[56] In comparison, the C_2H_4 uptake of HOF-NBDA at 10 kPa and 298 K is only 0.3 mmol g^{-1}, which is much lower than the corresponding uptake of C_3H_6. Under these conditions, the absorption ratio of C_3H_6 to C_2H_4 can be as high as 10.5 (Figure 2e). This significant difference in the adsorption capacity for C_3H_6 and C_2H_4 at low pressure indicates that the framework may have a higher affinity for C_3H_6, which benefits the C_2H_4/C_3H_6 separation. Another feature of HOF-NBDA is that the uptakes of C_3H_6 have no obvious decrease when raising the temperature. Even at 328 K, for HOF-NBDA, the C_3H_6 uptake is still up to 4.6 mmol g^{-1}. The high uptakes at high temperatures promise good C_2H_4/C_3H_6 separation potential over a wide temperature range.

To further assess the different adsorption behaviors of C_3H_6 and C_2H_4, the heat of adsorption (Q_{st}) was calculated using the adsorption isotherms. As depicted in Figures S1 and S2 and Table S1, the Q_{st} value for C_3H_6 at zero coverage is 25.7 kJ mol^{-1}, which is much higher than that for C_2H_4 (18.8 kJ mol^{-1}), suggesting that HOF-NBDA exhibits certainly stronger affinity for C_3H_6 and shows great potential for the efficient separation of C_3H_6 and C_2H_4. Even more interestingly, as for HOF-NBDA, the Q_{st} for C_3H_6 is indeed lower than those of all other C_3H_6-selective materials, such as zeolite 4A (29.9 kJ mol^{-1}),[57] HOF-ZSTU-2a (38.1 kJ mol^{-1}),[58] CR-COF-1 (29.0 kJ mol^{-1}),[37] and iso-MOF-4 (30.9 kJ mol^{-1}),[55] and only slightly higher than its vaporation enthalpy of 18.5 kJ mol^{-1}.[59] This moderate Q_{st} value for C_3H_6 indicates the feasibility of easy regeneration of HOF-NBDA in an ambient environment, and the adsorbed C_3H_6 in a fixed bed can be desorbed under much more mild conditions.[60] To further evaluate the separation ability of the HOF-NBDA for C_2H_4/C_3H_6, an ideal adsorbed solution theory (IAST) calculation was employed on the base of the single-component C_3H_6 and C_2H_4 adsorption isotherms at 298 K. As shown in Figures 2d and 2e, as well as Table S1, the IAST selectivity for $C_2H_4/$

https://doi.org/10.1021/acsmaterialslett.4c00111
ACS Materials Lett. 2024, 6, 1388−1395

C_3H_6 with the ratio of 50/50 (v/v) can climb to 11.1 as the pressure rises to 1.0 bar, which is only lower than that of $Zn_2(oba)_2(dmimpym)$ (15.6),[52] which is the reported highest value to date. This result confirms the excellent preferential capture ability of C_3H_6 over C_2H_4 in the separation process. More importantly, with the temperature gradually increasing, there is no significant decrease in C_2H_4/C_3H_6 selectivity. And even when the temperature reaches 328 K, the selectivity remains 8.0. The result above indicates that HOF-NBDA has an excellent C_2H_4/C_3H_6 separation potential. Considering its actual application, the repeatability and stability of HOF-NBDA were also tested through C_3H_6 adsorption experiments. As demonstrated in Figure 2f, after five adsorption cycles, or exposing the as-synthesized samples in air, water, and boiling water for 7 days, or activating the sample under 200 °C, the C_3H_6 adsorption isotherms still correspond well to the fresh HOF-NBDA, indicating the good stability and potential application for HOF-NBDA. Moreover, the water adsorption isotherm shows HOF-NBDA hardly adsorb water molecules when reaching the saturated vapor pressure (Figure S3), indicating that HOF-NBDA is not permeable to water.

To gain structural insights into the host−guest interactions between HOF-NBDA and the gas molecules and to investigate the mechanism of gas adsorption and separation potential in depth, we performed theoretical calculations to determine the adsorption sites of C_2H_4 and C_3H_6 in the framework. As shown in Figure 3a, the C_2H_4 molecule is slightly tilted in the pores of

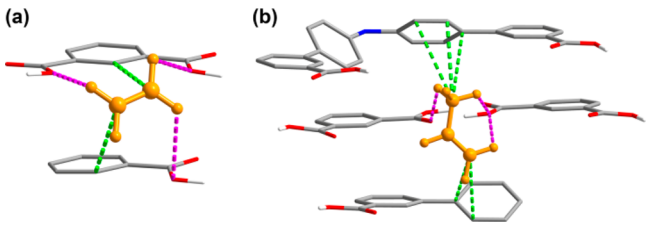

Figure 3. Calculated optimized adsorption sites for (a) C_2H_4 and (b) C_3H_6 in HOF-NBDA. (Legend: C, gray; O, red; N, blue; H, white.) The C−H···O interactions are shown as dashed purple lines, and the C···C separations between the gas molecule and the pore surface are shown as dashed green lines interactions). For clarity, C_2H_4 and C_3H_6 molecules are shown in orange, and the H atoms in benzene rings are omitted.

HOF-NBDA and interacted with two adjacent layers of skeleton through two C−H···π (corresponding C···C separations, 3.88 and 3.98 Å, respectively) and three C−H···O (H···O distances, 2.88, 2.90, and 2.92 Å, respectively) interactions. The corresponding calculated static binding energy is 31.0 kJ mol^{-1}. Similar to C_2H_4, the C_3H_6 molecule is also laying on the pore surface. However, with a larger molecular size, C_3H_6 could interact with the adjacent three-layer framework (Figure 3b). Moreover, the methyl groups of C_3H_6 are close to two layers of the framework, contributing to the formation of multiple van der Waals interactions. The C_3H_6 molecule interacted with the two nearest phenyl rings and two carboxylic acids through five C−H···π and three C−H···O interactions (corresponding C···C separations, 3.73, 3.76, 3.96, 3.98, and 4.05 Å and H···O distances, 2.74, 2.89, and 2.99 Å, respectively). The corresponding static binding energy for C_3H_6 is 38.4 kJ mol^{-1}, much higher than that for C_2H_4. These results comprehensively indicate that the nonpolar pore surface and two-dimensional layered structure of HOF-NBDA are undoubtedly beneficial for capturing C_3H_6 from C_2H_4/C_3H_6 mixtures.

Transient breakthrough simulations were conducted for HOF-NBDA in a packed column to determine the feasibility of MTO product separation. As shown in Figure S4, efficient separation can be accomplished by HOF-NBDA for C_2H_4/C_3H_6 (50/50, v/v), wherein C_2H_4 breakthrough occurs first and C_3H_6 passes through the fixed bed after a certain time. Next, we conducted dynamic breakthrough experiments with a C_2H_4/C_3H_6 mixture (50/50, v/v) under various conditions. As shown in Figure 4a, at 298 K with a flow rate of 1.7 mL min^{-1}, C_2H_4 passes through the packed column at first at 60.5 min g^{-1} and the C_3H_6 gas is not detected until 147.4 min g^{-1}. Therefore, high-purity C_2H_4 (≥99.95%) can be obtained for a long period of 86.9 min g^{-1}. There is an excellent match between the experimental and simulated breakthrough curves (Figure S4). The calculated C_2H_4 productivity is 5.7 mol kg^{-1}, which is the highest value and superior to that of all promising porous materials for C_2H_4/C_3H_6 separation to date, such as $Zn_2(oba)_2(dmimpym)$ (1.6 mol kg^{-1}), Mn-dtzip (1.2 mol kg^{-1}), Zn-BPZ-SA (1.0 mol kg^{-1}), and Zn-BPZ-TATB (4.5 mol kg^{-1})[61] (see Table S2). In addition, after five cycling experiments, or exposing HOF-NBDA to the atmosphere for five weeks, no obvious changes in retention time were observed (see Figure 4a, as well as Figure S5), simultaneously indicating that HOF-NBDA performs good reusability for C_2H_4/C_3H_6 separation. To further verify that HOF-NBDA can work well under the actual conditions, we also investigated the C_2H_4/C_3H_6 separation performance at different gas flow rates (2.5, 3.4, 4.2, and 5.0 mL min^{-1}) and under different temperatures (303, 308, 318, and 328 K). It can be seen from Figures 4b and 4c that the flow rates have little effect on the separation performance. At flow rates of 2.5, 3.4, 4.2, and 5.0 mL min^{-1}, the separation time is 54.1, 41.5, 31.4, and 26.3 min g^{-1}, respectively, and the corresponding C_2H_4 productivity is 5.6, 5.6, 5.6, and 5.5 mol kg^{-1}, respectively (see Table S3). When the temperature reaches 303, 308, 318, and 328 K, the corresponding C_2H_4 productivity is 5.2, 5.1, 5.0, and 4.6 mol kg^{-1}, respectively (Table S4). Furthermore, given good water resistance and the unavoidability of water vapor in the environment,[62−64] we also tested the C_2H_4/C_3H_6 separation performance of HOF-NBDA under different humidity conditions. As shown in Figure 4d, the separation performance only shows a slight decline in the relative humidity (RH) range of 33%−100%.

Desorption experiments were also conducted to evaluate C_3H_6 productivity. It is noteworthy that benefiting from the moderate interactions between the C_3H_6 and framework, the adsorbed C_3H_6 in the fixed bed can be completely purged out with He flow (flow rate = 15 mL min^{-1}) at room temperature within 2 h. As depicted in Figures S6 and S7, when the He flow was switched into the fixed bed, a small amount of C_2H_4 was eluted quickly. Then high-purity C_3H_6 (≥99.5%) could be continuously collected. After one circle of desorption test,~4.5 mol kg^{-1} of polymer-grade C_3H_6 could be obtained. Furthermore, corresponding desorption experiments were also performed when the breakthrough tests were handled under different conditions. The various test results shown in Figures S8−S29 and Tables S3−S5 indicate that the flow rate, humidity, and temperature have a minimal effect on the desorption results. These results show that HOF-NBDA exhibits superior C_2H_4/C_3H_6 separation performance.

https://doi.org/10.1021/acsmaterialslett.4c00111
ACS Materials Lett. 2024, 6, 1388−1395

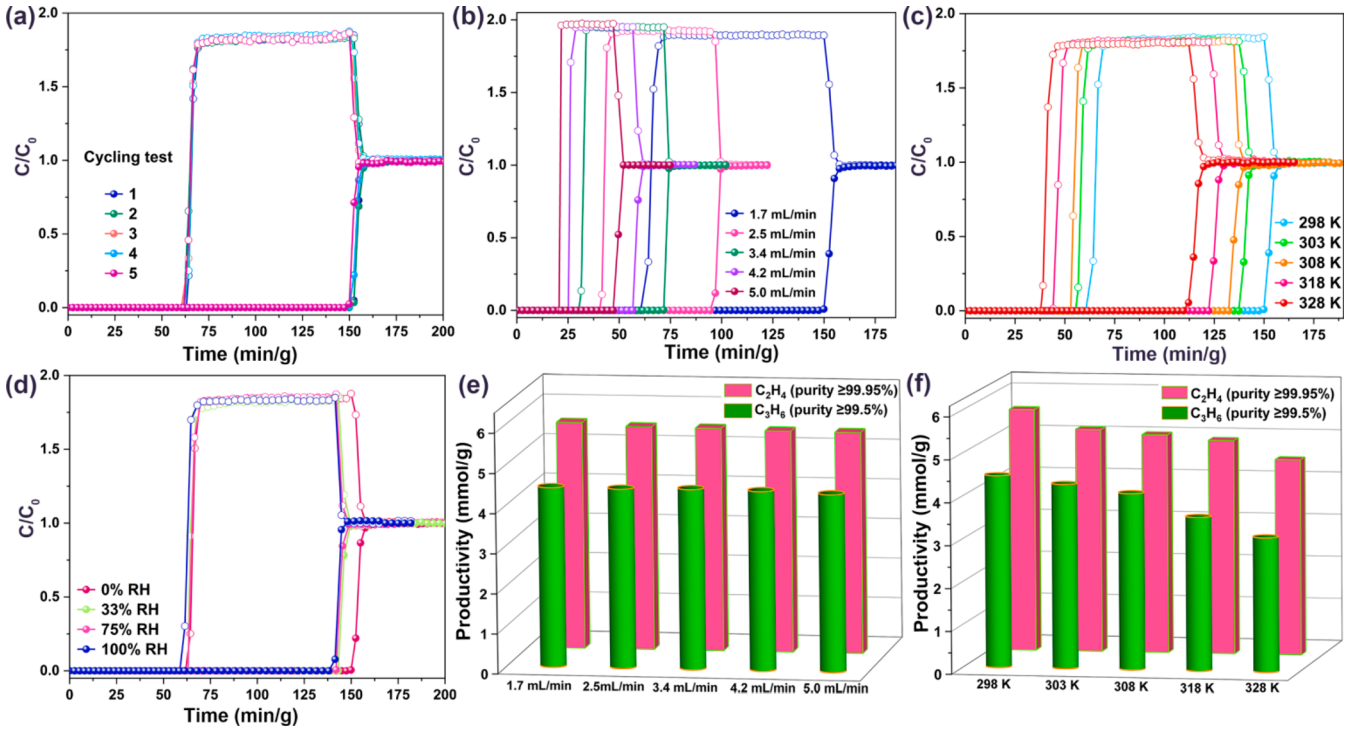

Figure 4. Breakthrough experiments of HOF-NBDA for C_2H_4/C_3H_6 (50/50, v/v). (a) Cycling breakthrough tests of HOF-NBDA for C_2H_4/C_3H_6 with a flow rate of 1.7 mL min^{-1}. (b) Separation experiments of HOF-NBDA at different gas flow rates at a temperature of 298 K. (c) Separation experiments of HOF-NBDA under different temperatures with a gas flow rate of 1.7 mL min^{-1}. (d) The breakthrough experiments of HOF-NBDA at different relative humidities with a gas flow rate of 1.7 mL min^{-1} and a temperature of 298 K. (e) Comparation of the productivities for C_2H_4 and C_3H_6 under different flow rates in break-through experiments at 298 K. (f) Comparation of the productivities for C_2H_4 and C_3H_6 at different temperatures with a flow rate of 1.7 mL min^{-1}.

Considering the real industrial applications, an ideal adsorbent should have some other characteristics besides good separation potential, such as excellent stability, easy scalability of synthesis, and good regeneration performance. For HOF-NBDA, a simple method can be employed for its synthesis on a large scale (see the Supporting Information and Figure S30). Furthermore, injured HOF-NBDA can be redissolved in a solvent of DMF, and only if poor solvents like methanol are added to it, the fresh HOF-NBDA can be regenerated with a yield of more than 98%. PXRD and the C_3H_6 adsorption curve indicated that the regenerated HOF-NBDA had excellent crystallinity and porosity (see Figures S31 and S33). Taken as a whole, HOF-NBDA meets almost all of the criteria required for industrial adsorbents, which is quite different from some benchmark materials that have been reported, rendering that HOF-NBDA has the potential to serve as a practical method for C_2H_4/C_3H_6 separation.

In summary, we have reported a porous layered hydrogen-bonded organic framework HOF-NBDA, which provides a C_3H_6 preferred pore environment. The significant difference in the uptakes of C_3H_6 and C_2H_4, especially at low pressure, endows it with the second-highest C_2H_4/C_3H_6 IAST selectivity. The above result indicates that there are stronger interactions between C_3H_6 and the pore, which also has been demonstrated by the theoretical calculation. Practical breakthrough experiments under ambient conditions show that polymer-grade C_2H_4 and C_3H_6 can be obtained in the separation and desorption process from the mixture of C_2H_4/C_3H_6 (50/50, v/v). More importantly, after one circle of breakthrough experiments, record-high productivities of C_2H_4 and C_3H_6 could also be directly obtained, i.e., 5.7 mol kg^{-1} C_2H_4 with a purity of >99.95% and 4.5 mol kg^{-1} C_3H_6 with a purity of >99.5%. Additionally, HOF-NBDA retains good C_2H_4/C_3H_6 separation performance at different gas flow rates, temperatures, and relative humidities, which has rarely been seen in the C_2H_4/C_3H_6 separation materials previously. These results indicate that HOF-NBDA can achieve efficient C_3H_6/C_2H_4 separation and potentially purify MTO products. This work illustrates the importance of the layered hydrogen-bonded organic frameworks in promoting the separation of gas mixtures, as well as the viable prospect of HOF as the separation materials, which provide guidance for the design of highly efficient and regeneratable materials for MTO product separation in the future.

■ ASSOCIATED CONTENT

Supporting Information

The Supporting Information is available free of charge at https://pubs.acs.org/doi/10.1021/acsmaterialslett.4c00111.

Materials and instrumentation; scale-up synthesis of HOF-NBDA; regeneration of HOF-NBDA; gas sorption experiments; calculation of isosteric enthalpy of adsorption (Q_{st}); calculation of selectivity via IAST; computational details; transient breakthrough simulations; column breakthrough experiments; various supplemental figures and tables; associated references (PDF)

https://doi.org/10.1021/acsmaterialslett.4c00111
ACS Materials Lett. 2024, 6, 1388−1395

AUTHOR INFORMATION

Corresponding Author

Mingyan Wu − *State Key Laboratory of Structure Chemistry, Fujian Institute of Research on the Structure of Matter, Chinese Academy of Sciences, Fuzhou 350002 Fujian, China; University of Chinese Academy of Sciences, Beijing 100049, China;* orcid.org/0000-0003-2610-285X; Email: wumy@fjirsm.ac.cn

Authors

Yunzhe Zhou − *State Key Laboratory of Structure Chemistry, Fujian Institute of Research on the Structure of Matter, Chinese Academy of Sciences, Fuzhou 350002 Fujian, China; Fujian College, University of Chinese Academy of Sciences, Fuzhou 350002 Fujian, China*

Cheng Chen − *State Key Laboratory of Structure Chemistry, Fujian Institute of Research on the Structure of Matter, Chinese Academy of Sciences, Fuzhou 350002 Fujian, China; Fujian College, University of Chinese Academy of Sciences, Fuzhou 350002 Fujian, China*

Zhenyu Ji − *State Key Laboratory of Structure Chemistry, Fujian Institute of Research on the Structure of Matter, Chinese Academy of Sciences, Fuzhou 350002 Fujian, China*

Rajamani Krishna − *Van 't Hoff Institute for Molecular Sciences, University of Amsterdam, 1098 XH Amsterdam, The Netherlands;* orcid.org/0000-0002-4784-8530

Zhengyi Di − *State Key Laboratory of Structure Chemistry, Fujian Institute of Research on the Structure of Matter, Chinese Academy of Sciences, Fuzhou 350002 Fujian, China*

Daqiang Yuan − *State Key Laboratory of Structure Chemistry, Fujian Institute of Research on the Structure of Matter, Chinese Academy of Sciences, Fuzhou 350002 Fujian, China;* orcid.org/0000-0003-4627-072X

Complete contact information is available at: https://pubs.acs.org/10.1021/acsmaterialslett.4c00111

Author Contributions

Mingyan Wu and Yunzhe Zhou proposed the ideas and supervised the project. Yunzhe Zhou and Cheng Chen synthesized the HOFs and conducted their characterization. Zhenyu Ji performed gas sorption and separation experiments. Daqiang Yuan and Rajamani Krishna conducted the theoretical calculations. Mingyan Wu and Yunzhe Zhou analyzed data and wrote the manuscript. All authors discussed the results and commented on the manuscript.

Notes

The authors declare no competing financial interest.

ACKNOWLEDGMENTS

This work is supported by NSFC (No. 22271282) and the Self-Deployment Project Research Program of Haixi Institutes, Chinese Academy of Sciences (through Grant No. CXZX-2022-JQ04). Additionally, this work is also supported by Fujian Science & Technology Innovation Laboratory for Optoelectronic Information of China (No. 2021ZR120) and NSF of Fujian Province (Nos. 2021J01517 and 2020J06034).

REFERENCES

(1) Adil, K.; Belmabkhout, Y.; Pillai, R. S.; Cadiau, A.; Bhatt, P. M.; Assen, A. H.; Maurin, G.; Eddaoudi, M. Gas/Vapour Separation using Ultra-Microporous Metal-Organic Frameworks: Insights into the Structure/Separation Relationship. *Chem. Soc. Rev.* **2017**, *46*, 3402−3430.

(2) Yang, L.; Qian, S.; Wang, X.; Cui, X.; Chen, B.; Xing, H. Energy-Efficient Separation Alternatives: Metal-Organic Frameworks and Membranes for Hydrocarbon Separation. *Chem. Soc. Rev.* **2020**, *49*, 5359−5406.

(3) Lin, R.-B.; Xiang, S.; Zhou, W.; Chen, B. Microporous Metal-Organic Framework Materials for Gas Separation. *Chem.* **2020**, *6*, 337−363.

(4) Di, Z.; Liu, C.; Pang, J.; Zou, S.; Ji, Z.; Hu, F.; Chen, C.; Yuan, D.; Hong, M.; Wu, M. A Metal-Organic Framework with Nonpolar Pore Surfaces for the One-step Acquisition of C_2H_4 from a C_2H_4 and C_2H_6 Mixture. *Angew. Chem., Int. Ed.* **2022**, *61*, No. e202210343.

(5) Ke, T.; Wang, Q.; Shen, J.; Zhou, J.; Bao, Z.; Yang, Q.; Ren, Q. Molecular Sieving of C-2−C-3 Alkene from Alkyne with Tuned Threshold Pressure in Robust Layered Metal-Organic Frameworks. *Angew. Chem., Int. Ed.* **2020**, *59*, 12725−12730.

(6) Wang, Y.; Li, T.; Li, L.; Lin, R.-B.; Jia, X.; Chang, Z.; Wen, H.-M.; Chen, X.-M.; Li, J. Construction of Fluorinated Propane-Trap in Metal-Organic Frameworks for Record Polymer-Grade Propylene Production under High Humidity Conditions. *Adv. Mater.* **2023**, *35*, 2207955.

(7) Zeng, H.; Xie, M.; Wang, T.; Wei, R.-J.; Xie, X.-J.; Zhao, Y.; Lu, W.; Li, D. Orthogonal-Array Dynamic Molecular Sieving of Propylene/Propane Mixtures. *Nature* **2021**, *595*, 542−548.

(8) Pang, J.; Ma, Z.; Yang, Q.; Zhang, K.; Lian, X.; Huang, H.; Yao, Z.; Li, B.; Xu, J.; Bu, X. A highly connected metal-organic framework with a specific nonpolar nanotrap for inverse ethane/ethylene separation. *Inorg. Chem. Front.* **2023**, *10*, 6407−6413.

(9) Ding, Q.; Zhang, Z.; Liu, Y.; Chai, K.; Krishna, R.; Zhang, S. One-Step Ethylene Purification from Ternary Mixtures in a Metal-Organic Framework with Customized Pore Chemistry and Shape. *Angew. Chem., Int. Ed.* **2022**, *61*, No. e202208134.

(10) Tian, P.; Wei, Y.; Ye, M.; Liu, Z. Methanol to Olefins (MTO): From Fundamentals to Commercialization. *ACS Catal.* **2015**, *5*, 1922−1938.

(11) Yang, M.; Fan, D.; Wei, Y.; Tian, P.; Liu, Z. Recent Progress in Methanol-to-Olefins (MTO) Catalysts. *Adv. Mater.* **2019**, *31*, 1902181.

(12) Wang, C.; Yang, L.; Gao, M.; Shao, X.; Dai, W.; Wu, G.; Guan, N.; Xu, Z.; Ye, M.; Li, L. Directional Construction of Active Naphthalenic Species within SAPO-34 Crystals toward More Efficient Methanol-to-Olefin Conversion. *J. Am. Chem. Soc.* **2022**, *144*, 21408−21416.

(13) Cesarini, A.; Mitchell, S.; Zichittella, G.; Agrachev, M.; Schmid, S. P.; Jeschke, G.; Pan, Z.; Bodi, A.; Hemberger, P.; Perez-Ramirez, J. Elucidation of Radical- and Oxygenate-Driven Paths in Zeolite-Catalysed Conversion of Methanol and Methyl Chloride to Hydrocarbons. *Nat. Catal.* **2022**, *5*, 605−614.

(14) Yarulina, I.; De Wispelaere, K.; Bailleul, S.; Goetze, J.; Radersma, M.; Abou-Hamad, E.; Vollmer, I.; Goesten, M.; Mezari, B.; Hensen, E. J. M.; Martinez-Espin, J. S.; Morten, M.; Mitchell, S.; Perez-Ramirez, J.; Olsbye, U.; Weckhuysen, B. M.; Van Speybroeck, V.; Kapteijn, F.; Gascon, J. Structure-Performance Descriptors and the Role of Lewis Acidity in the Methanol-to-Propylene Process. *Nat. Chem.* **2018**, *10*, 804−812.

(15) Belohlav, Z.; Zamostny, P.; Herink, T. The Kinetic Model of Thermal Cracking for Olefins Production. *Chem. Eng. Process.* **2003**, *42*, 461−473.

(16) Wang, J.-X.; Liang, C.-C.; Gu, X.-W.; Wen, H.-M.; Jiang, C.; Li, B.; Qian, G.; Chen, B. Recent Advances in Microporous Metal-Organic Frameworks as Promising Adsorbents for Gas Separation. *J. Mater. Chem. A* **2022**, *10*, 17878−17916.

(17) Wang, J.; Lian, X.; Zhang, Z.; Liu, X.; Zhao, Q.; Xu, J.; Cao, X.; Li, B.; Bu, X. Thiazole Functionalized Covalent Triazine Frameworks for C_2H_6/C_2H_4 Separation with Remarkable Ethane Uptake. *Chem. Commun.* **2023**, *59*, 11240−11243.

(18) Peng, Y.-L.; Pham, T.; Li, P.; Wang, T.; Chen, Y.; Chen, K.-J.; Forrest, K. A.; Space, B.; Cheng, P.; Zaworotko, M. J.; Zhang, Z. Robust Ultramicroporous Metal-Organic Frameworks with Bench-

mark Affinity for Acetylene. *Angew. Chem., Int. Ed.* **2018**, *57*, 10971−10975.
(19) Di, Z.; Liu, C.; Pang, J.; Chen, C.; Hu, F.; Yuan, D.; Wu, M.; Hong, M. Cage-Like Porous Materials with Simultaneous High C_2H_2 Storage and Excellent C_2H_2/CO_2 Separation Performance. *Angew. Chem., Int. Ed.* **2021**, *60*, 10828−10832.
(20) Dong, Q.; Huang, Y.; Wan, J.; Lu, Z.; Wang, Z.; Gu, C.; Duan, J.; Bai, J. Confining Water Nanotubes in a $Cu_{10}O_{13}$-Based Metal-Organic Framework for Propylene/Propane Separation with Record-High Selectivity. *J. Am. Chem. Soc.* **2023**, *145*, 8043−8051.
(21) Zhou, D.; Zhang, J. On the Role of Flexibility for Adsorptive Separation. *Acc. Chem. Res.* **2022**, *55*, 2966−2977.
(22) Tang, Y.; Wang, Z.; Yi, H.; Zhou, M.; Zhou, D.; Zhang, J.; Chen, X. Water-Stable Metal Azolate Frameworks Showing Interesting Flexibilities for Highly Effective Bioethanol Dehydration. *Angew. Chem., Int. Ed.* **2023**, *62*, No. e202303374.
(23) Wu, F.; Li, L.; Tan, Y.; El-Sayed, E.-S. M.; Yuan, D. The Competitive and Synergistic Effect Between Adsorption Enthalpy and Capacity in D_2/H_2 Separation of M_2(m-dobdc) Frameworks. *Chin. Chem. Lett.* **2021**, *32*, 3562−3565.
(24) Zhang, L.; Ma, L.-N.; Wang, G.-D.; Hou, L.; Zhu, Z.; Wang, Y.-Y. A New Honeycomb MOF for C_2H_4 Purification and C_3H_6 Enrichment by Separating Methanol to Olefin Products. *J. Mater. Chem. A* **2023**, *11*, 2343−2348.
(25) Wang, G.-D.; Krishna, R.; Li, Y.-Z.; Ma, Y.-Y.; Hou, L.; Wang, Y.-Y.; Zhu, Z. Rational Construction of Ultrahigh Thermal Stable MOF for Efficient Separation of MTO Products and Natural Gas. *ACS Mater. Lett.* **2023**, *5*, 1091−1099.
(26) Fang, H.; Zheng, B.; Zhang, Z. H.; Li, H. X.; Xue, D. X.; Bai, J. Ligand-Conformer-Induced Formation of Zirconium-Organic Framework for Methane Storage and MTO Product Separation. *Angew. Chem., Int. Ed.* **2021**, *60*, 16521−16528.
(27) Li, J.-R.; Kuppler, R. J.; Zhou, H.-C. Selective Gas Adsorption and Separation in Metal-Organic Frameworks. *Chem. Soc. Rev.* **2009**, *38*, 1477−1504.
(28) Song, X.; Wang, Y.; Wang, C.; Wang, D.; Zhuang, G.; Kirlikovali, K. O.; Li, P.; Farha, O. K. Design Rules of Hydrogen-Bonded Organic Frameworks with High Chemical and Thermal Stabilities. *J. Am. Chem. Soc.* **2022**, *144*, 10663−10687.
(29) Hisaki, I.; Xin, C.; Takahashi, K.; Nakamura, T. Designing Hydrogen-Bonded Organic Frameworks (HOFs) with Permanent Porosity. *Angew. Chem., Int. Ed.* **2019**, *58*, 11160−11170.
(30) Liu, J.; Miao, J.; Ullah, S.; Zhou, K.; Yu, L.; Wang, H.; Wang, Y.; Thonhauser, T.; Li, J. A Water-Resistant Hydrogen-Bonded Organic Framework for Ethane/Ethylene Separation in Humid Environments. *ACS Mater. Lett.* **2022**, *4*, 1227−1232.
(31) Ye, Y.; Xie, Y.; Shi, Y.; Gong, L.; Phipps, J.; Al-Enizi, A. M.; Nafady, A.; Chen, B.; Ma, S. A Microporous Metal-Organic Framework with Unique Aromatic Pore Surfaces for High Performance C_2H_6/C_2H_4 Separation. *Angew. Chem., Int. Ed.* **2023**, *62*, 202302564.
(32) Zhang, X.; Li, L.; Wang, J.-X.; Wen, H.-M.; Krishna, R.; Wu, H.; Zhou, W.; Chen, Z.-N.; Li, B.; Qian, G.; Chen, B. Selective Ethane/Ethylene Separation in a Robust Microporous Hydrogen-Bonded Organic Framework. *J. Am. Chem. Soc.* **2020**, *142*, 633−640.
(33) Hashim, M. I.; Le, H. T. M.; Chen, T.-H.; Chen, Y.-S.; Daugulis, O.; Hsu, C.-W.; Jacobson, A. J.; Kaveevivitchai, W.; Liang, X.; Makarenko, T.; et al. Dissecting Porosity in Molecular Crystals: Influence of Geometry, Hydrogen Bonding, and [$\pi\cdots\pi$] Stacking on the Solid-State Packing of Fluorinated Aromatics. *J. Am. Chem. Soc.* **2018**, *140*, 6014−6026.
(34) Cui, P.; Svensson Grape, E.; Spackman, P. R.; Wu, Y.; Clowes, R.; Day, G. M.; Inge, A. K.; Little, M. A.; Cooper, A. I. An Expandable Hydrogen-Bonded Organic Framework Characterized by Three-Dimensional Electron Diffraction. *J. Am. Chem. Soc.* **2020**, *142*, 12743−12750.
(35) Suzuki, Y.; Tohnai, N.; Saeki, A.; Hisaki, I. Hydrogen-Bonded Organic Frameworks of Twisted Polycyclic Aromatic Hydrocarbon. *Chem. Commun.* **2020**, *56*, 13369−13372.
(36) Hisaki, I.; Suzuki, Y.; Gomez, E.; Ji, Q.; Tohnai, N.; Nakamura, T.; Douhal, A. Acid Responsive Hydrogen-Bonded Organic Frameworks. *J. Am. Chem. Soc.* **2019**, *141*, 2111−2121.
(37) Han, X. H.; Gong, K.; Huang, X.; Yang, J. W.; Feng, X.; Xie, J.; Wang, B. Syntheses of Covalent Organic Frameworks via a One-Pot Suzuki Coupling and Schiff's Base Reaction for C_2H_4/C_3H_6 Separation. *Angew. Chem., Int. Ed.* **2022**, *61*, No. e202202912.
(38) Jiang, L.; Tian, Y.; Sun, T.; Zhu, Y.; Ren, H.; Zou, X.; Ma, Y.; Meihaus, K. R.; Long, J. R.; Zhu, G. A Crystalline Polyimide Porous Organic Framework for Selective Adsorption of Acetylene over Ethylene. *J. Am. Chem. Soc.* **2018**, *140*, 15724−15730.
(39) Wen, H.-M.; Yu, C.; Liu, M.; Lin, C.; Zhao, B.; Wu, H.; Zhou, W.; Chen, B.; Hu, J. Construction of Negative Electrostatic Pore Environments in a Scalable, Stable and Low-Cost Metal-Organic Framework for One-Step Ethylene Purification from Ternary Mixtures. *Angew. Chem., Int. Ed.* **2023**, *62*, No. e202309108.
(40) Gao, J.; Cai, Y.; Qian, X.; Liu, P.; Wu, H.; Zhou, W.; Liu, D.-X.; Li, L.; Lin, R.-B.; Chen, B. A Microporous Hydrogen-Bonded Organic Framework for the Efficient Capture and Purification of Propylene. *Angew. Chem., Int. Ed.* **2021**, *60*, 20400−20406.
(41) Lin, R.-B.; Li, L.; Zhou, H.-L.; Wu, H.; He, C.; Li, S.; Krishna, R.; Li, J.; Zhou, W.; Chen, B. Molecular Sieving of Ethylene from Ethane Using a Rigid Metal-Organic Framework. *Nat. Mater.* **2018**, *17*, 1128.
(42) Zhou, Y.; Chen, C.; Krishna, R.; Ji, Z.; Yuan, D.; Wu, M. Tuning Pore Polarization to Boost Ethane/Ethylene Separation Performance in Hydrogen-Bonded Organic Frameworks. *Angew. Chem., Int. Ed.* **2023**, *62*, No. e202305041.
(43) Hu, F.; Liu, C.; Wu, M.; Pang, J.; Jiang, F.; Yuan, D.; Hong, M. h An Ultrastable and Easily Regenerated Hydrogen-Bonded Organic Molecular Framework with Permanent Porosity. *Angew. Chem., Int. Ed.* **2017**, *56*, 2101−2104.
(44) Yang, Y.; Li, L.; Lin, R.-B.; Ye, Y.; Yao, Z.; Yang, L.; Xiang, F.; Chen, S.; Zhang, Z.; Xiang, S.; Chen, B. Ethylene/Ethane Separation in a Stable Hydrogen-Bonded Organic Framework through a Gating Mechanism. *Nat. Chem.* **2021**, *13*, 933.
(45) Chen, S.; Ju, Y.; Zhang, H.; Zou, Y.; Lin, S.; Li, Y.; Wang, S.; Ma, E.; Deng, W.; Xiang, S.; Chen, B.; Zhang, Z. Photo Responsive Electron and Proton Conductivity within a Hydrogen-Bonded Organic Framework. *Angew. Chem., Int. Ed.* **2023**, *62*, No. e202308418.
(46) Zentner, C. A.; Lai, H. W. H.; Greenfield, J. T.; Wiscons, R. A.; Zeller, M.; Campana, C. F.; Talu, O.; FitzGerald, S. A.; Rowsell, J. L. C. High Surface Area and Z′ in a Thermally Stable 8-Fold Polycatenated Hydrogen-Bonded Framework. *Chem. Commun.* **2015**, *51*, 11642−11645.
(47) Li, Y. L.; Alexandrov, E. V.; Yin, Q.; Li, L.; Fang, Z. B.; Yuan, W.; Proserpio, D. M.; Liu, T. F. Record Complexity in the Polycatenation of Three Porous Hydrogen-Bonded Organic Frameworks with Stepwise Adsorption Behaviors. *J. Am. Chem. Soc.* **2020**, *142*, 7218−7224.
(48) Li, Y.; Wang, X.; Zhang, H.; He, L.; Huang, J.; Wei, W.; Yuan, Z.; Xiong, Z.; Chen, H.; Xiang, S.; Chen, B.; Zhang, Z. A Microporous Hydrogen Bonded Organic Framework for Highly Selective Separation of Carbon Dioxide over Acetylene. *Angew. Chem., Int. Ed.* **2023**, *62*, No. e202311419.
(49) Herbstein, F. H.; Kapon, M.; Reisner, G. M. Catenated and Non-Catenated Inclusion Complexes of Trimesic Acid. *Journal of Inclusion Phenomena* **1987**, *5*, 211−214.
(50) Vishweshwar, P.; Beauchamp, D. A.; Zaworotko, M. J. An Acetic Acid Solvate of Trimesic Acid that Exhibits Triple Inclined Interpenetration and Mixed Supramolecular Homosynthons. *Cryst. Growth Des.* **2006**, *6*, 2429−2431.
(51) Duchamp, D. J.; Marsh, R. E. Crystal Structure of Trimesic Acid (Benzene-1,3,5-Tricarboxylic Acid). *Acta Crystallogr., Sect. B: Struct. Crystallogr. Cryst. Chem.* **1969**, *25*, 5−19.
(52) Li, Y.-Z.; Wang, G.-D.; Krishna, R.; Yin, Q.; Zhao, D.; Qi, J.; Sui, Y.; Hou, L. A Separation MOF with O/N Active Sites in

Nonpolar Pore for One-step C_2H_4 Purification from C_2H_6 or C_3H_6 Mixtures. *Chem. Eng. J.* **2023**, *466*, 143056.
(53) Fan, W.; Wang, Y.; Zhang, Q.; Kirchon, A.; Xiao, Z.; Zhang, L.; Dai, F.; Wang, R.; Sun, D. An Amino-Functionalized Metal-Organic Framework, Based on a Rare $Ba_{12}(COO)_{18}(NO_3)_2$ Cluster, for Efficient C3/C2/C1 Separation and Preferential Catalytic Performance. *Chem.—Eur. J.* **2018**, *24*, 2137−2143.
(54) Liu, X.; Hao, C.; Li, J.; Wang, Y.; Hou, Y.; Li, X.; Zhao, L.; Zhu, H.; Guo, W. An Anionic Metal-Organic Framework: Metathesis of Zinc(ii) with Copper(ii) for Efficient C3/C2 Hydrocarbon and Organic Dye Separation. *Inorg. Chem. Front* **2018**, *5*, 2898−2905.
(55) Fan, W.; Wang, X.; Zhang, X.; Liu, X.; Wang, Y.; Kang, Z.; Dai, F.; Xu, B.; Wang, R.; Sun, D. Fine-Tuning the Pore Environment of the Microporous Cu-MOF for High Propylene Storage and Efficient Separation of Light Hydrocarbons. *ACS Central Sci.* **2019**, *5*, 1261−1268.
(56) Zhang, L.; Ma, L.-N.; Wang, G.-D.; Hou, L.; Zhu, Z.; Wang, Y.-Y. A New Honeycomb MOF for C_2H_4 Purification and C_3H_6 Enrichment by Separating Methanol to Olefin Products. *J. Mater. Chem. A* **2023**, *11*, 2343−2348.
(57) Da Silva, F. A.; Rodrigues, A. E. Adsorption Equilibria and Kinetics for Propylene and Propane over 13X and 4A Zeolite Pellets. *Ind. Eng. Chem. Res.* **1999**, *38*, 2051−2057.
(58) Cai, Y.; Gao, J.; Li, J.-H.; Liu, P.; Zheng, Y.; Zhou, W.; Wu, H.; Li, L.; Lin, R.-B.; Chen, B. Pore Modulation of Hydrogen-Bonded Organic Frameworks for Efficient Separation of Propylene. *Angew. Chem., Int. Ed.* **2023**, *62*, No. e202308579.
(59) Chickos, J. S.; Acree, W. E. Enthalpies of Vaporization of Organic and Organometallic Compounds, 1880−2002. *J. Phys. Chem. Ref. Data* **2003**, *32*, 519−878.
(60) Huang, X.; Jiang, S.; Ma, D.; Xie, J.; Feng, X.; Wang, B. Molecular Exclusion Separation of 1-Butene Isomers by a Robust Metal-Organic Framework under Humid Conditions. *Angew. Chem., Int. Ed.* **2023**, *62*, No. e202303671.
(61) Wang, G.-D.; Li, Y.-Z.; Shi, W.-J.; Hou, L.; Wang, Y.-Y.; Zhu, Z. Active Sites Decorated Nonpolar Pore-Based MOF for One-step Acquisition of C_2H_4 and Recovery of C_3H_6. *Angew. Chem., Int. Ed.* **2023**, *62*, No. e202311654.
(62) Liu, Y.; Li, H.; Zou, S.; Di, Z.; Chen, C.; Wu, M.; Hong, M. Exceptionally Water-Stable In(III)-Based Framework with Conjugated Rhombohedral Cavities for Efficiently Separating Humid Flue Gas. *ACS Sustainable Chem. Eng.* **2022**, *10*, 15335−15343.
(63) Gan, L.; Andres-Garcia, E.; Minguez Espallargas, G.; Planas, J. G. Adsorptive Separation of CO_2 by a Hydrophobic Carborane-Based Metal-Organic Framework under Humid Conditions. *ACS Appl. Mater. Interfaces* **2023**, *15*, 5309−5316.
(64) Xie, X.-J.; Zeng, H.; Xie, M.; Chen, W.; Hua, G.-F.; Lu, W.; Li, D. A Metal-Organic Framework for C_2H_2/CO_2 Separation under Highly Humid Conditions: Balanced Hydrophilicity/Hydrophobicity. *Chem. Eng. J.* **2022**, *427*, 132033.

https://doi.org/10.1021/acsmaterialslett.4c00111
ACS Materials Lett. 2024, 6, 1388−1395

Supporting Information

A Layered Hydrogen-Bonded Organic Framework with C_3H_6-preferred Pores for Efficient One-step Purification of MTO Products

Yunzhe Zhou[1,2], Cheng Chen[1,2], Zhenyu Ji[1], Rajamani Krishna[3], Zhengyi Di[1], Daqiang Yuan[1] & Mingyan Wu[1,4]*

[1]State Key Lab of Structural Chemistry, Fujian Institute of Research on the Structure of Matter, Chinese Academy of Sciences, Fuzhou, Fujian, 350002, China

[2]Fujian College, University of Chinese Academy of Sciences, Fuzhou, Fujian, 350002, China

[3]Van 't Hoff Institute for Molecular Sciences, University of Amsterdam, Science Park 904, 1098 XH Amsterdam, The Netherlands

[4]University of Chinese Academy of Sciences, Beijing, 100049, China

* Correspondence and requests for materials should be addressed to M.W. (E-mail: wumy@fjirsm.ac.cn).

Materials and Instrumentation

Unless otherwise stated, all reagents and solvents used in studies were purchased from commercial sources and were used without further purification. Powder X-ray diffraction (PXRD) patterns were performed on a MiniFlex 600 diffractometer equipped using Cu Kα (λ = 1.5406 Å), scanning at 1°/min in a range of 4~50°. The thermogravimetric analysis (TGA) was performed on a NETZSCH STA 449C unit at a heating rate of 10 ℃·min^{-1} under nitrogen atmosphere. ^{1}H nuclear magnetic resonance (NMR) spectra was obtained on a Bruker AVANCE III 400 (400 MHz) spectrometer. Fourier transform infrared (FT-IR) spectra was obtained from 4000 to 400 cm^{-1} using a Vertex70 spectrometer with a Smart Golden Gate ATR attachment. Scanning electron microscopy (SEM) images were taken with a ZEISS SIGMA 300 microscope.

Scale-up synthesis of HOF-NBDA

To obtain a good deal of sample in one batch for adsorption and separation experiments, H_6NBDA (10.0 g, 13.5 mmol) was dissolved in 150 mL dry DMF in a beaker and the mixture was filtrated by a filter membrane (50 mm, 0.22 μm). Then 500 mL dry methanol was slowly added to the mixture with stirring, and yellow crystals were rapidly precipitated. The product was separated by suction filtration and further washed several times with methanol, which can be characterized by PXRD patterns.[1]

Regeneration of HOF-NBDA

The damaged sample can be easily reproduced by dissolving in DMF solution.[1]

Gas sorption experiments

All gas adsorption measurements were measured on Micromeritics 3Flex. The fresh sample of HOF-NBDA was exchanged with dry methanol for 7 days. Then the sample was evacuated at ambient temperature for 10 h and subsequently 373 K for 10 h until the outgas rate was 5 μmHg min^{-1} before measurement. Guest-free HOF-NBDA was transferred to Micromeritics 3Flex to experiment. The sorption experiments were maintained at 77 K with liquid nitrogen or under 273 - 328 K in a water bath. Water adsorption isotherm was measured using a Bel Japan Inc. model BELSOPR-Max analyzer at 298 K. The sample was activated at 373 K under vacuum for 10 h before the analysis was started.

Calculation of isosteric enthalpy of adsorption (Q_{st})

The isosteric enthalpies of adsorption for C_3H_6 and C_2H_4 were calculated using the isotherms at 298 K, 308 K and 318 K were fitted to a virial equation (Eqn (1)). The fitting parameters were then used to calculate the isosteric heat of adsorption (Q_{st}) using Eqn (2).

$$\ln P = \ln N + \frac{1}{T}\sum_{i=0}^{m} a_i N^i + \sum_{i=0}^{n} b_i N^i \qquad (1)$$

$$Q_{st} = -R\sum_{i=0}^{m} a_i N^i \qquad (2)$$

where P is the pressure (mmHg), N is the adsorbed quantity (mmol·g^{-1}), T is the temperature (K), R is the gas constant (8.314 J·K^{-1}·mol^{-1}), a_i and b_i are virial coefficients required to detailed describe the isotherms, and m and n represent the number of coefficients required to adequately describe the isotherms. The obtained Viral model fitting parameters for C_2H_4 and C_3H_6 adsorption isotherms of HOF-NBDA:

	Parameter	Value	Standard Deviation		Parameter	Value	Standard Deviation
C_3H_6	a_0	-3.097754E+3	1.980164E+2	**C_2H_4**	a_0	-2.26683E+3	3.305805E+1
	a_1	2.033683E+0	5.556653E+0		a_1	-3.135850E+0	2.743241E+0
	a_2	-4.483549E-2	4.519638E-2		a_2	8.004988E-2	5.354565E-2
	a_3	-3.568750E-5	3.915081E-4		a_3	-2.750922E-3	1.159499E-3
	a_4	2.720613E-7	1.901894E-6		a_4	3.573652E-5	1.60819E-5
	a_5	5.345503E-10	3.321541E-9		a_5	-1.623249E-7	7.814944E-8
	b_0	9.759127E+0	6.374390E-1		b_0	9.705288E+0	1.073082E-1
	b_1	-9.945533E-3	1.711595E-2		b_1	5.201098E-3	8.923776E-3
	b_2	1.651870E-4	7.985172E-5		b_2	5.798322E-5	1.482136E-4
	R^2	0.99990			R^2	0.99997	

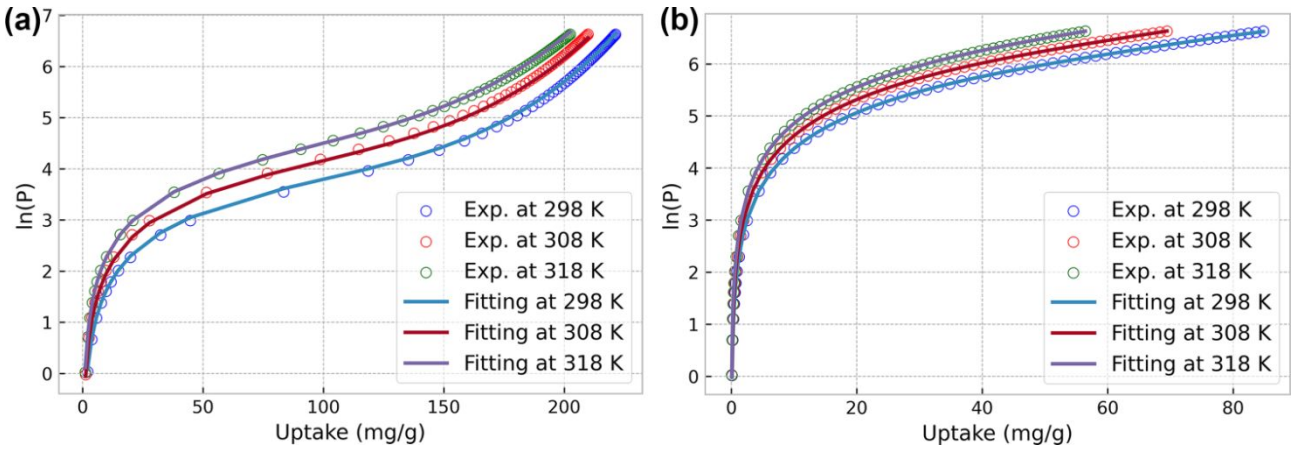

Figure S1. Viral equation fits (lines) of the HOF-NBDA **(a)** C_3H_6 and **(b)** C_2H_4 adsorption isotherms (points) measured at 298 K, 308 K and 318 K.

Calculation of selectivity via IAST

Single-component gas equilibrium adsorption isotherms were fitted with dual-site Langmuir–Freundlich (DSLF) model, given by the following equation:

$$N = A_1\frac{b_1 p^{c_1}}{1 + b_1 p^{c_1}} + A_2\frac{b_2 p^{c_2}}{1 + b_2 p^{c_2}} \qquad (3)$$

where N is the amount of adsorbed gas (mmol·g^{-1}), p is the bulk gas phase pressure (atm), A_1 and A_2 are the adsorption saturation capacity for site 1 and site 2 (mmol·g^{-1}), b_1 and b_2 are the affinity coefficients of site (1/kPa), c_1 and c_2 are the Langmuir–Freundlich exponent (dimensionless) for two adsorption sites A and B indicating the presence of weak and strong adsorption sites.

The parameters of A_1, A_2, b_1, b_2, and c_1, c_2 were then used to predict the adsorption selectivity based on IAST, which is finally defined as:

$$S_{\frac{1}{2}} = \left(\frac{x_1}{x_2}\right)\left(\frac{y_2}{y_1}\right) \qquad (4)$$

In equation (4), S is the ideal selectivity of component 1 over component 2, where x_i and y_i are the mole fractions of component i (i = 1 and 2) in the adsorbed and bulk phases, respectively. Dual-site Langmuir-Freundlich parameter fits for C_3H_6 and C_2H_4 in HOF-NBDA. The fits are based on experimental isotherm data at 298 K:

	$q_{sat,A}$	b_A	v_A	$q_{sat,B}$	b_B	v_B	R-Square
	cm^3·g^{-1}	kPa^{-1}	dimensionless	cm^3·g^{-1}	kPa^{-1}	dimensionless	
C_3H_6	2.95618 ±0.02854	0.09383 ±0.002	0.72251 ±0.01547	3.13814 ±0.06866	0.03276 ±0.00131	2.06977 ±0.02836	0.99999
C_2H_4	4.46848 ±0.20183	4.1512E-4 ±6.05363E-5	1.68367 ±0.03217	1.13758 ±0.17345	0.02815 ±0.00398	1.00749 ±0.00482	0.99999

Computational details

The binding sites for C_3H_6 and C_2H_4 in HOF-NBDA were determined through classical molecular simulations. The single X-ray crystallographic structures were subject to geometry optimization through the Dmol3 module implemented with the Materials Studio program, using the generalized gradient approximation (GGA) with the Perdew-Burke-Ernzerhof (PBE) functional and the double numerical plus d-functions (DNP) basis set. The energy, force, and displacement convergence criteria were set as 1×10^{-5} Ha, 2×10^{-3} Ha/Å and 5×10^{-3} Å, respectively. The calculated electrostatic potential for HOF-NBDA was mapped onto the Connolly surface with a probe radius of 1.0 Å. Simulated annealing (SA) calculations were performed for a single molecule of C_3H_6 and C_2H_4 through a canonical Monte Carlo (NVT) process, and all HOF atoms were kept fixed at their positions throughout the simulations. The initial configurations were further optimized to ensure a more efficient energy landscape scanning for every HOF-C_xH_x complex, and the optimized configuration having the lowest energy was used as the global minimum for the subsequent analysis and calculation. The static binding energy (at T= 0 K) was then calculated: $\triangle E = E_{HOF} + E_{gas} - E_{HOF+gas}$.

Transient breakthrough simulations

Transient breakthrough experiments were carried out for binary 50/50 $C_2H_4(1)/C_3H_6(2)$ mixtures at a total pressure of 0.16 MPa and 298 K. The sample mass of HOF in the packed bed, m_{ads} is 0.7936 g. The flow rates at the inlet, Q_0 = 1.7 mL·min^{-1}. Transient breakthrough simulations were carried out for the exact same set of operating conditions as in the experiments, using the methodology described in earlier publications[2-7]. In these simulations, intra-crystalline diffusion influences are ignored. There is good match between the experiments and simulations.

Column breakthrough experiments

The breakthrough separation experiments of HOF-NBDA for C_2H_4/C_3H_6 (50/50, v/v) were conducted in a fixed bed under ambient conditions. The mass of HOF-NBDA that was fed into the column (4.0 × 200 mm) was 0.7936 g. The flow rate of the gas was regulated by a mass flow controller, and the gas flow out of the chromatographic column was detected by a gas chromatography (GC) with TCD detector. Before breakthrough experiments, HOF-NBDA in the column was activated for 10 hours at 80°C with continuous He input (flow rate = 15 mL·min^{-1}). After the column was cooled to room temperture, C_2H_4/C_3H_6 gas mixture with a specific flow rate was switched into the column. The gas flow at the outlet of fixed bed was detected by a gas chromatography with TCD detector. When

the mixture of C_2H_4 and C_3H_6 at the outlet reached equilibrium, He flow (flow rate = 15 mL·min^{-1}) was purged out into the fixed bed contained HOF-NBDA at room temperature. The adsorbed gases in the fixed bed could be completely eluted out and the HOF-NBDA could realize regeneration in this progress. Desorption experiments were performed after C_2H_4/C_3H_6 equilibrated at the outlet. When the mixture was equilibrated, the breakthrough column was maintained at room temperature. And then He was purged (flow rate = 15 mL·min^{-1}). Therefore, desorption progress could be realized. In desorption tests, outlet gas from the column were continuously monitored by gas chromatography for determining the gas composition and purity.

Additional experimental details, supplementary data, and photograph of material objects:

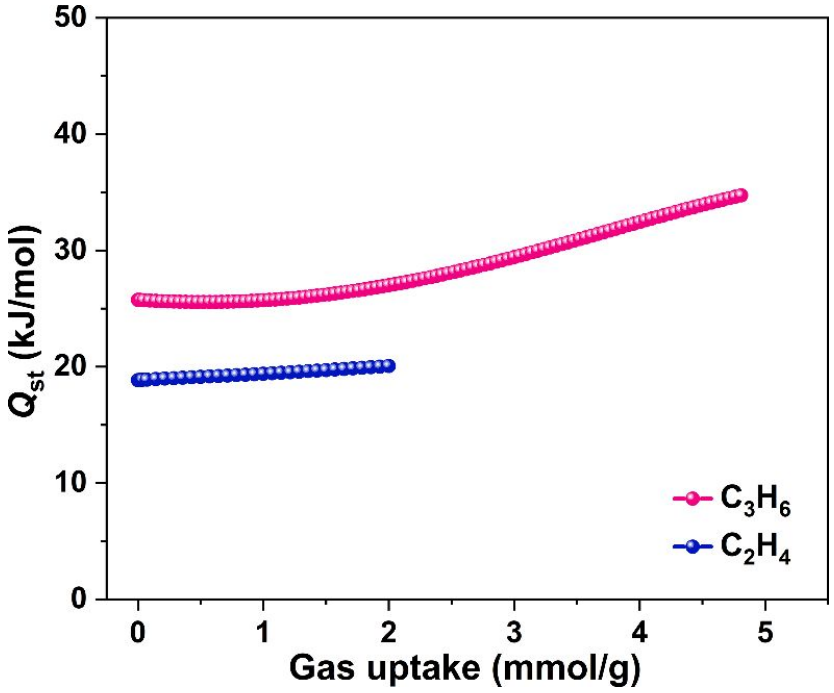

Figure S2. Calculated isosteric heats of adsorption of C_3H_6 and C_2H_4 in HOF-NBDA.

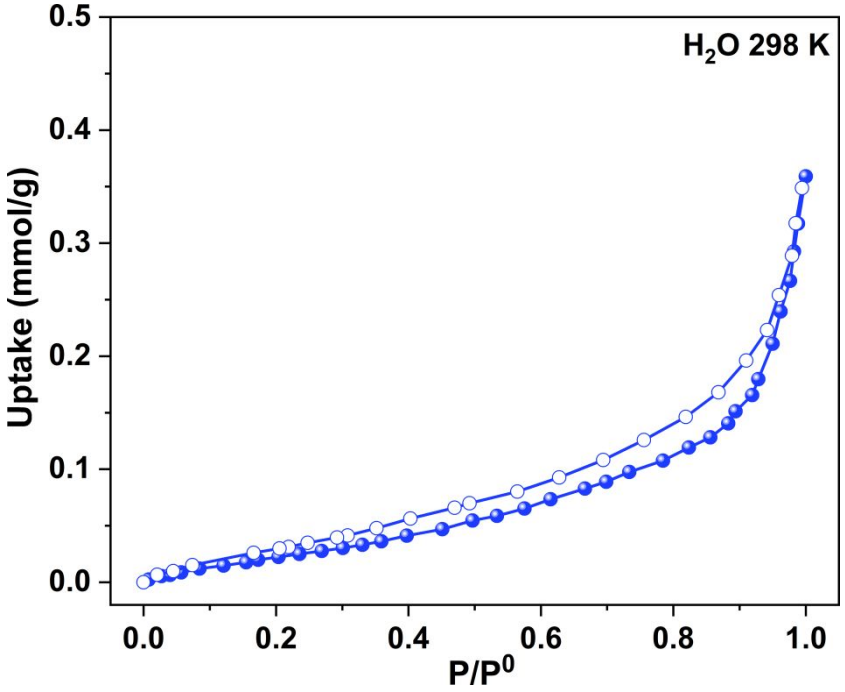

Figure S3. Water vapor adsorption isotherm of HOF-NBDA at 298 K.

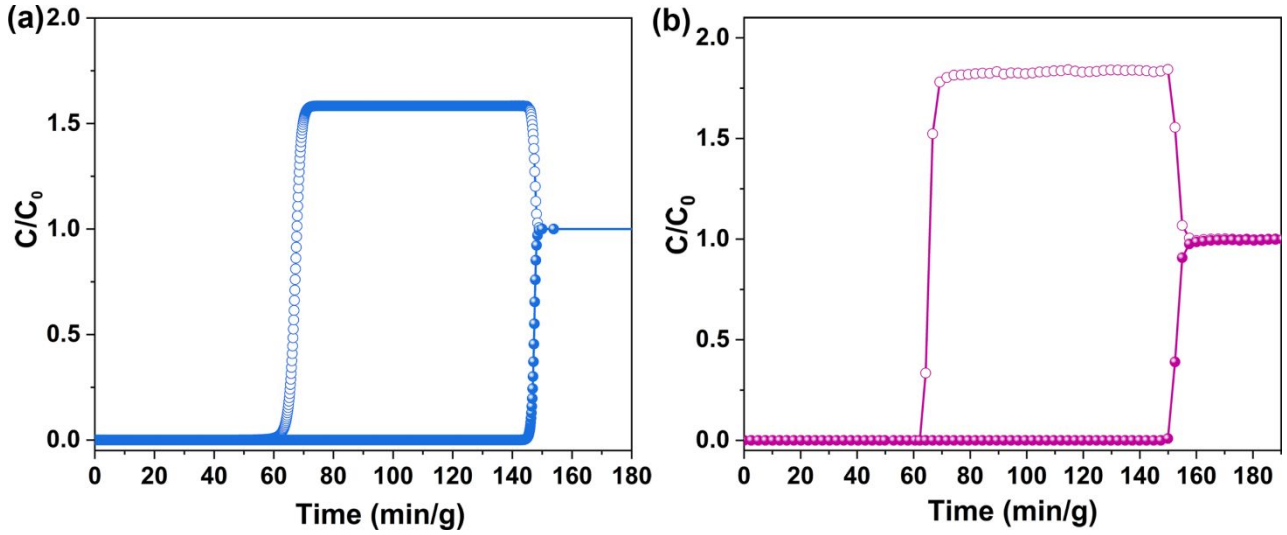

Figure S4. (a) The simulated and (b) experimental breakthrough curves of **HOF-NBDA** for C_2H_4/C_3H_6 (50/50, v/v) mixture with gas flow rate of the 1.7 mL·min^{-1} at 298 K.

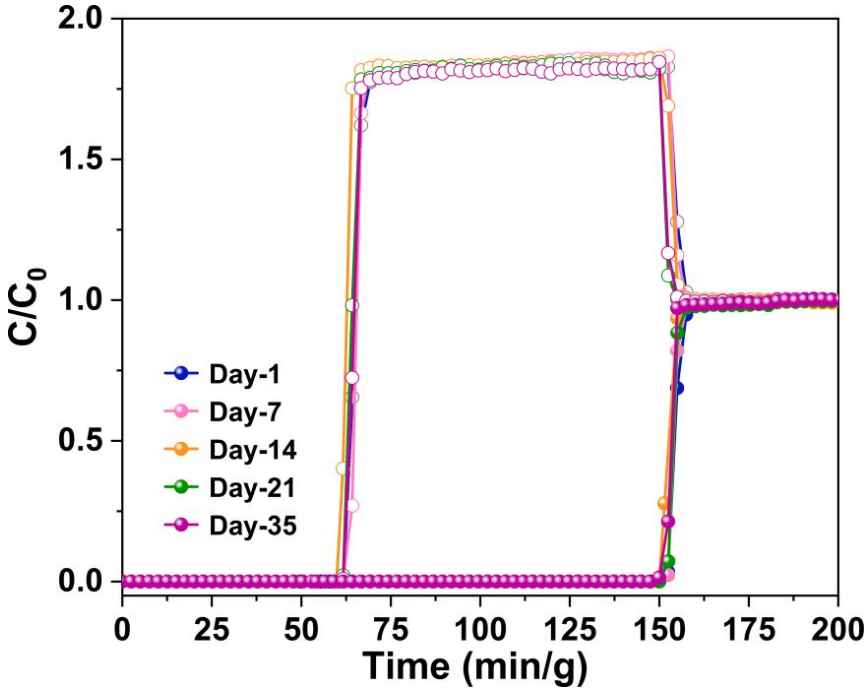

Figure S5. The breakthrough experiments of HOF-NBDA for C_2H_4/C_3H_6 (50/50, v/v) after one day, one week to five weeks with a flow rate of 1.7 mL·min^{-1} at 298 K, respectively.

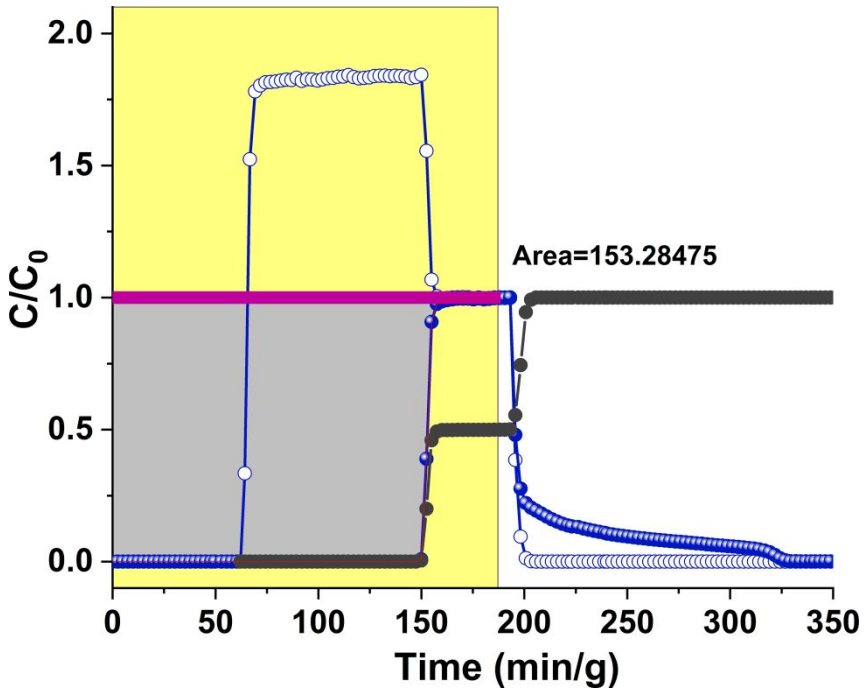

Figure S6. The adsorption capacity of C_3H_6 during the breakthrough process with flow rate of 1.7 mL·min^{-1} at 298 K.

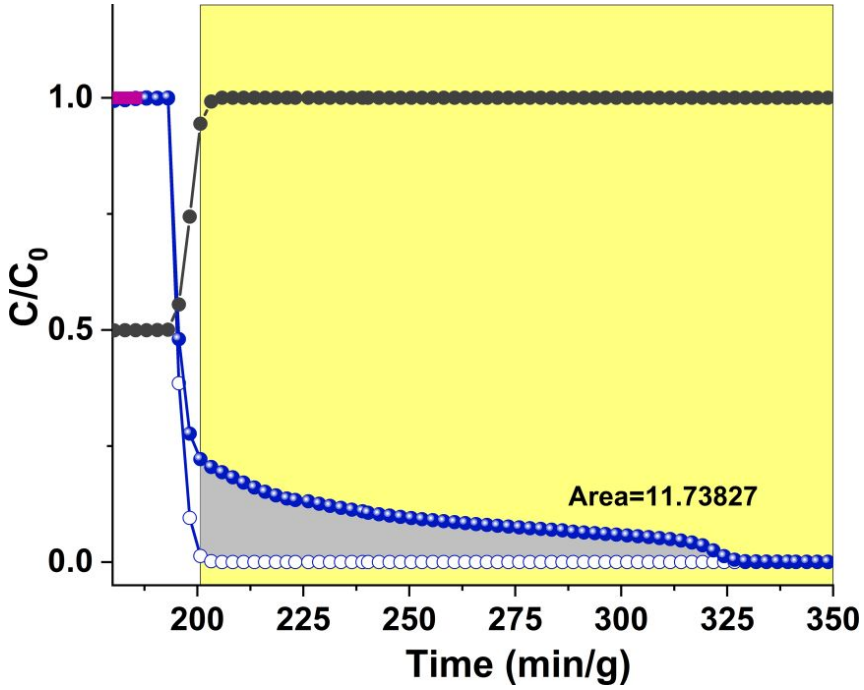

Figure S7. The C_3H_6 recovery of 4.5 mol·kg^{-1} with purity ≥99.5% during desorption process with flow rate of 1.7 mL·min^{-1} at 298 K.

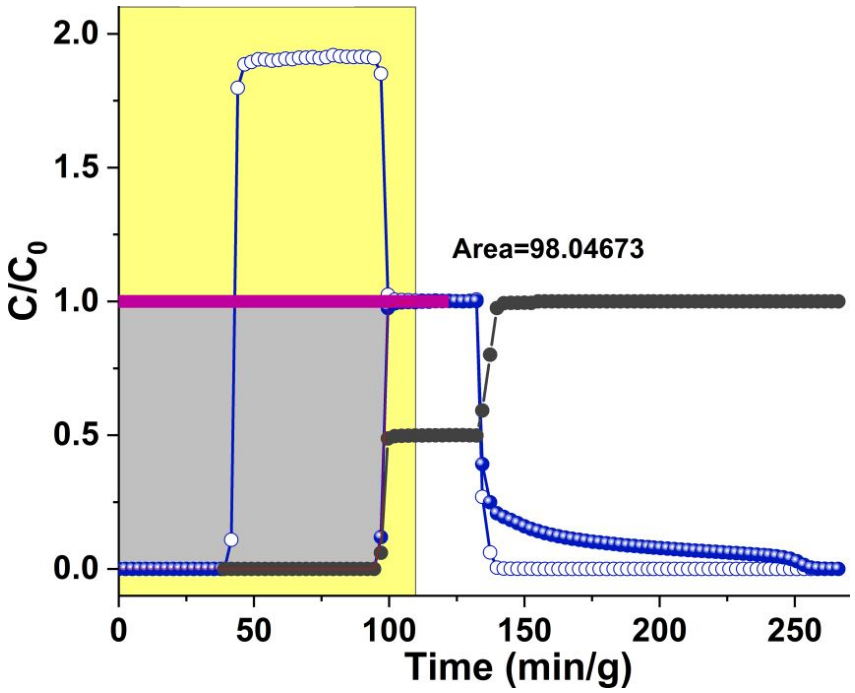

Figure S8. The adsorption capacity of C_3H_6 during the breakthrough process with flow rate of 2.5 mL·min^{-1} at 298 K.

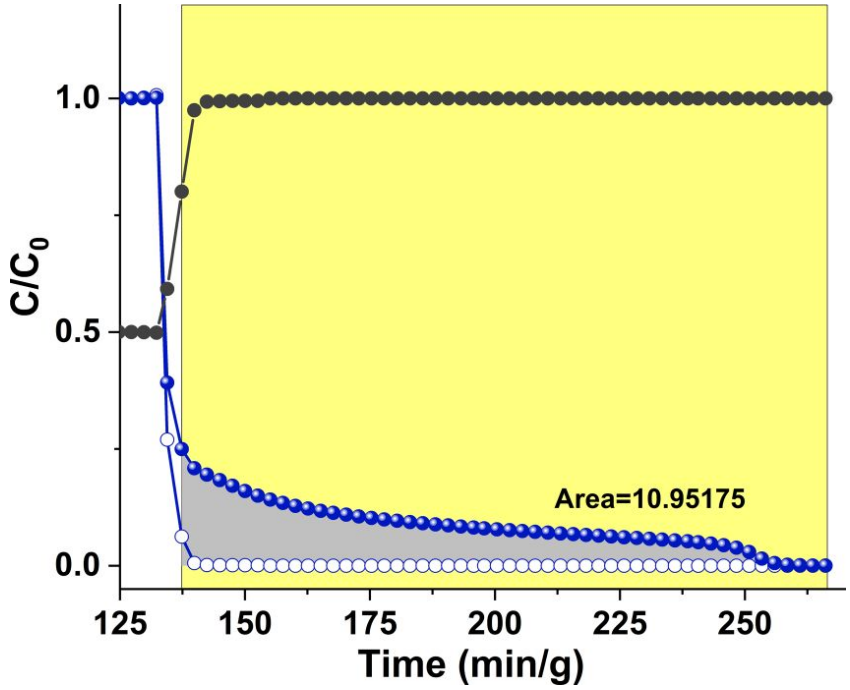

Figure S9. The C_3H_6 recovery of 4.5 mol·kg^{-1} with purity ≥99.5% during desorption process with flow rate of 2.5 mL·min^{-1} at 298 K.

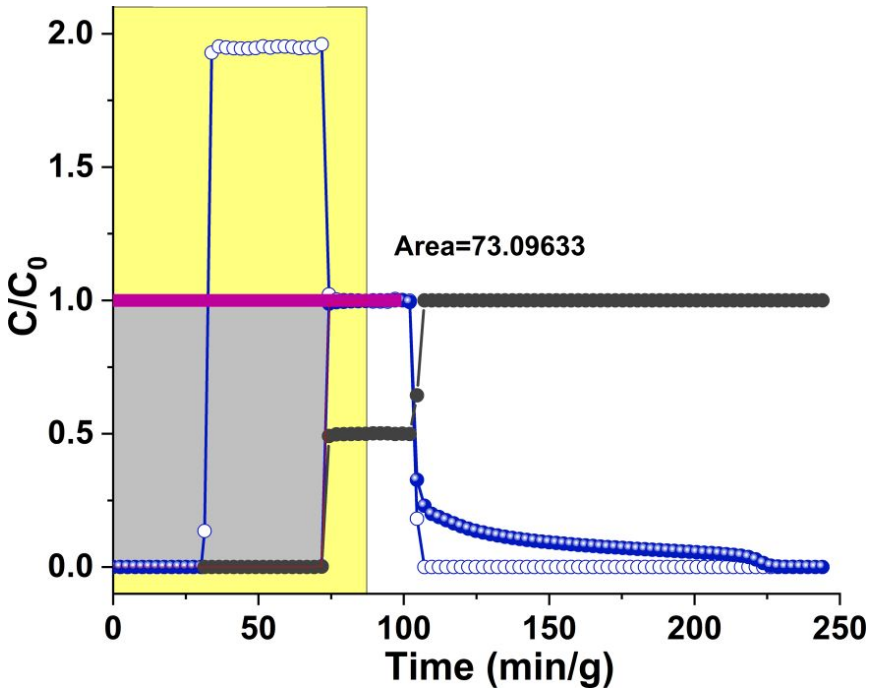

Figure S10. The adsorption capacity of C_3H_6 during the breakthrough process with flow rate of 3.4 mL·min^{-1} at 298 K.

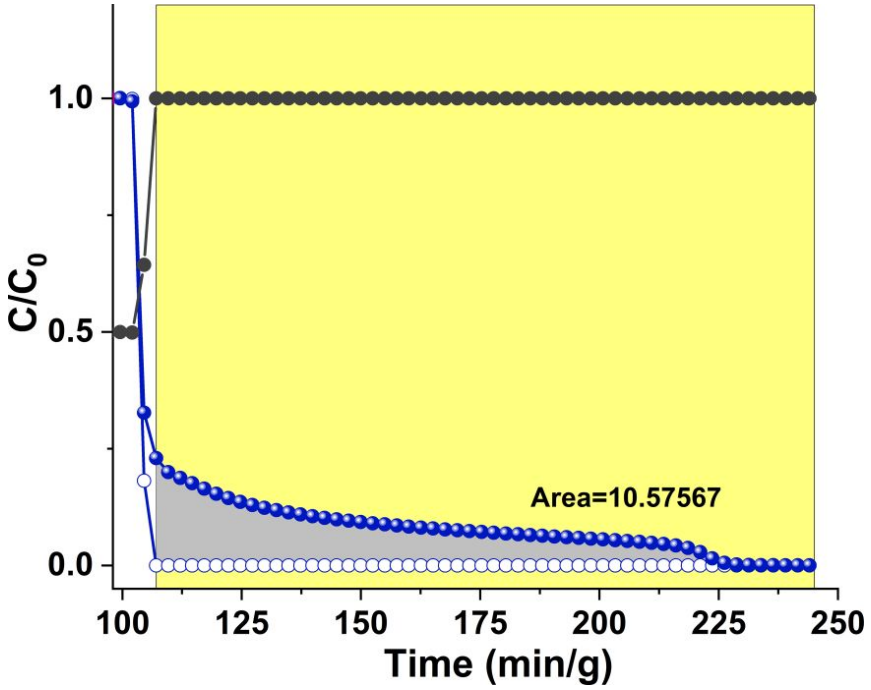

Figure S11. The C_3H_6 recovery of 4.5 mol·kg^{-1} with purity ≥99.5% during desorption process with flow rate of 3.4 mL·min^{-1} at 298 K.

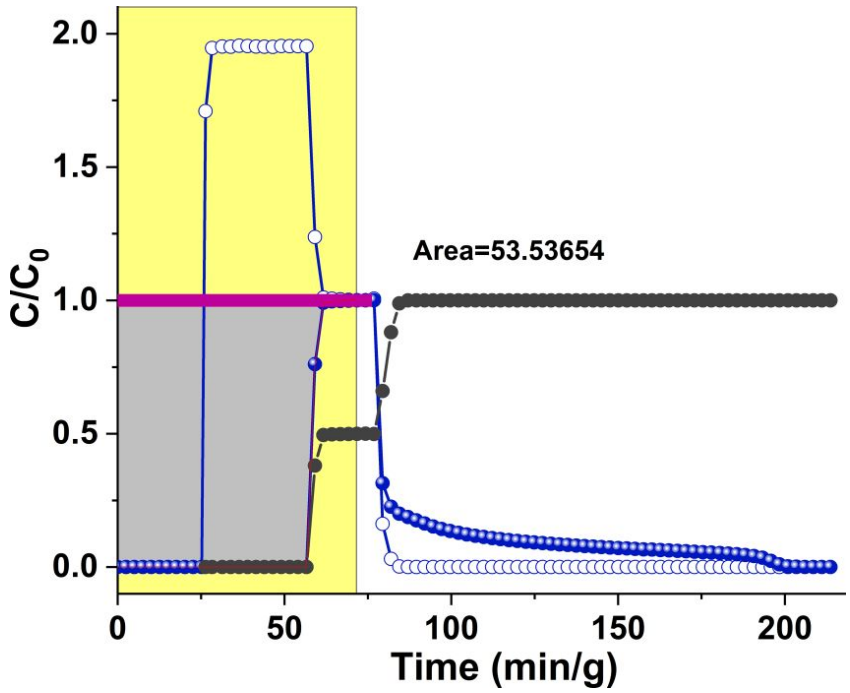

Figure S12. The adsorption capacity of C_3H_6 during the breakthrough process with flow rate of 4.2 $mL \cdot min^{-1}$ at 298 K.

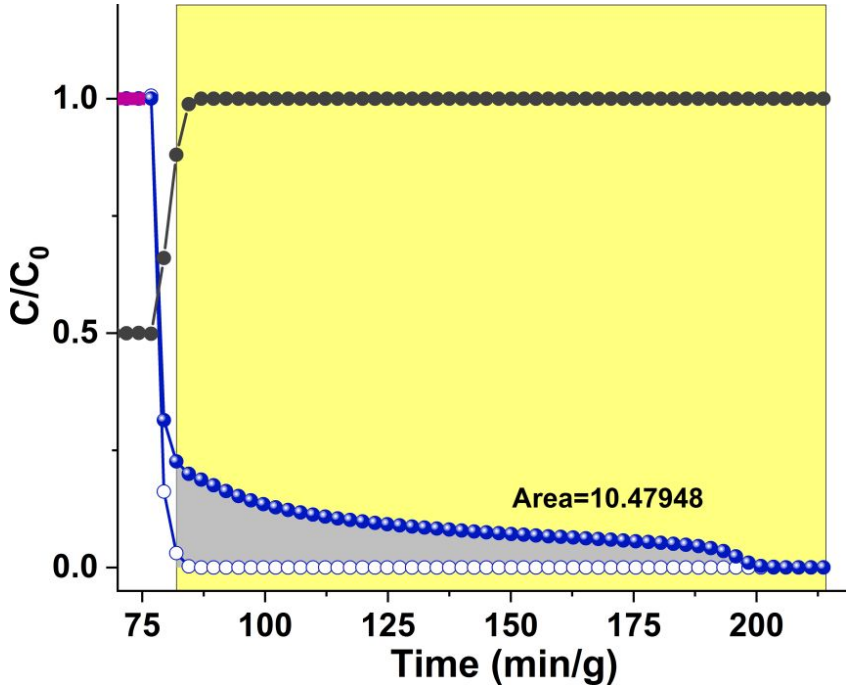

Figure S13. The C_3H_6 recovery of 4.5 $mol \cdot kg^{-1}$ with purity ≥99.5% during desorption process with flow rate of 4.2 $mL \cdot min^{-1}$ at 298 K.

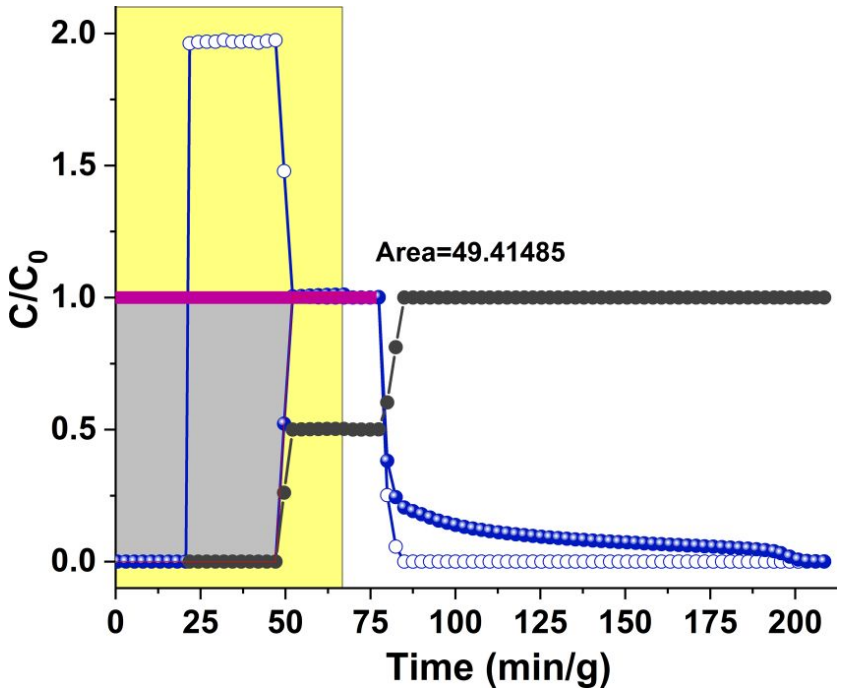

Figure S14. The adsorption capacity of C_3H_6 during the breakthrough process with flow rate of 5.0 mL·min^{-1} at 298 K.

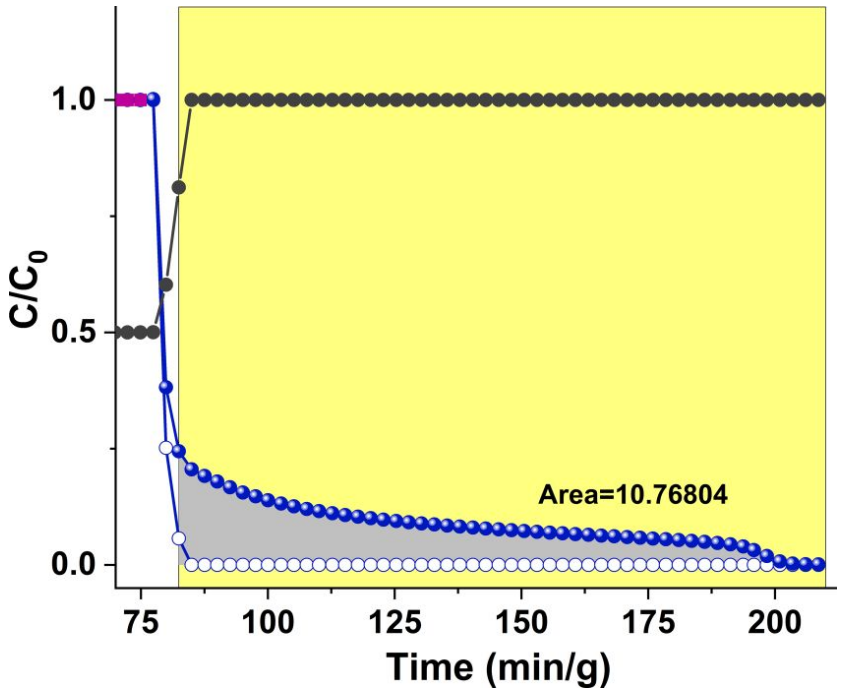

Figure S15. The C_3H_6 recovery of 4.4 mol·kg^{-1} with purity ≥99.5% during desorption process with flow rate of 5.0 mL·min^{-1} at 298 K.

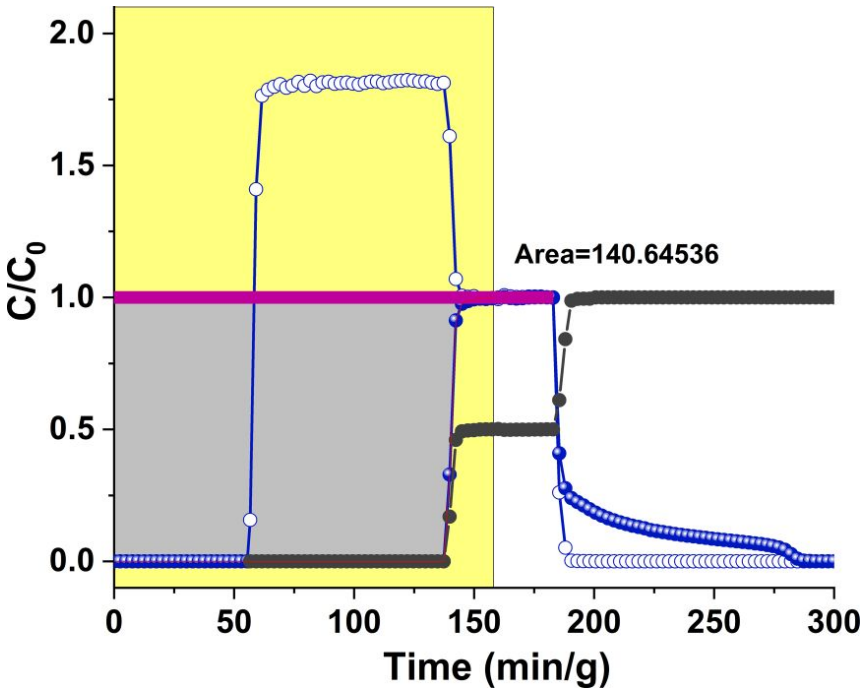

Figure S16. The adsorption capacity of C_3H_6 during the breakthrough process with flow rate of 1.7 $mL \cdot min^{-1}$ at 303 K.

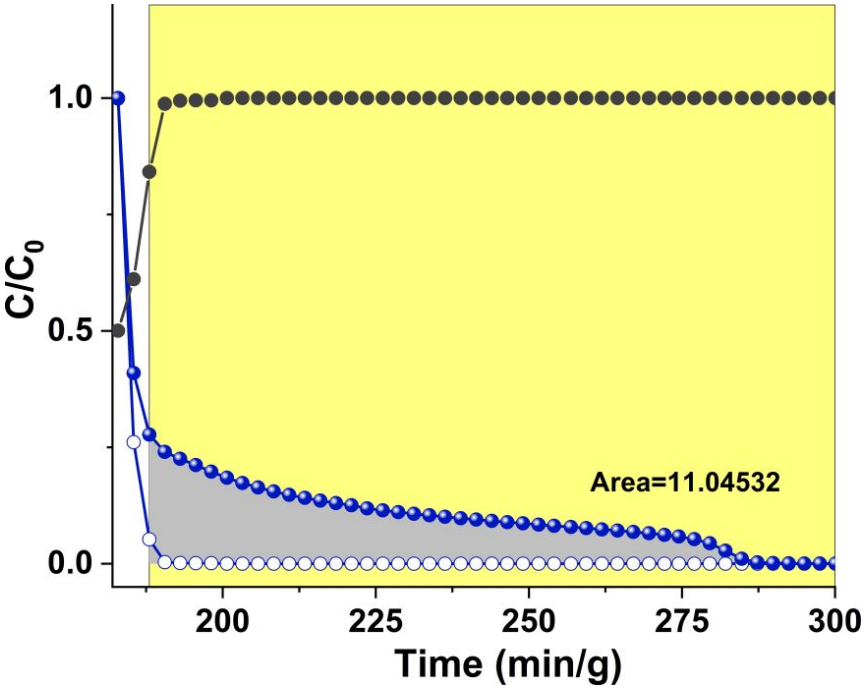

Figure S17. The C_3H_6 recovery of 4.3 $mol \cdot kg^{-1}$ with purity ≥99.5% during desorption process with flow rate of 1.7 $mL \cdot min^{-1}$ at 303 K.

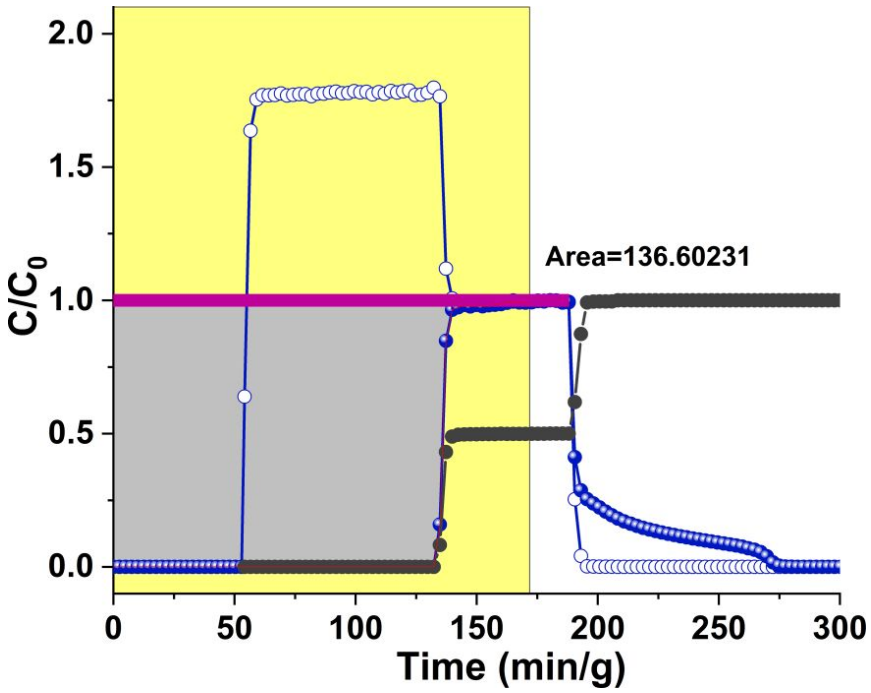

Figure S18. The adsorption capacity of C_3H_6 during the breakthrough process with flow rate of 1.7 mL·min^{-1} at 308 K.

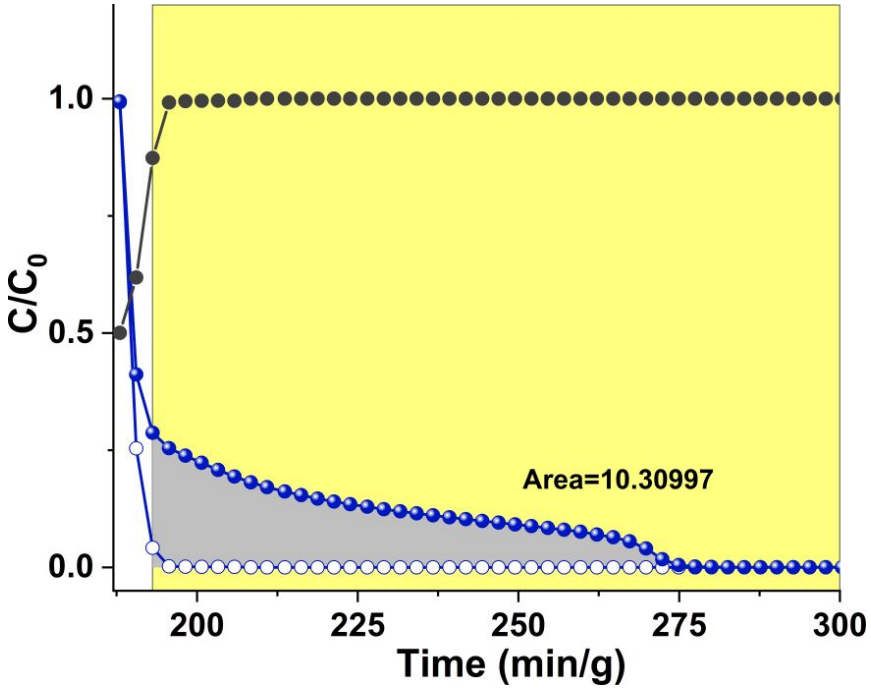

Figure S19. The C_3H_6 recovery of 4.1 mol·kg^{-1} with purity ≥99.5% during desorption process with flow rate of 1.7 mL·min^{-1} at 308 K.

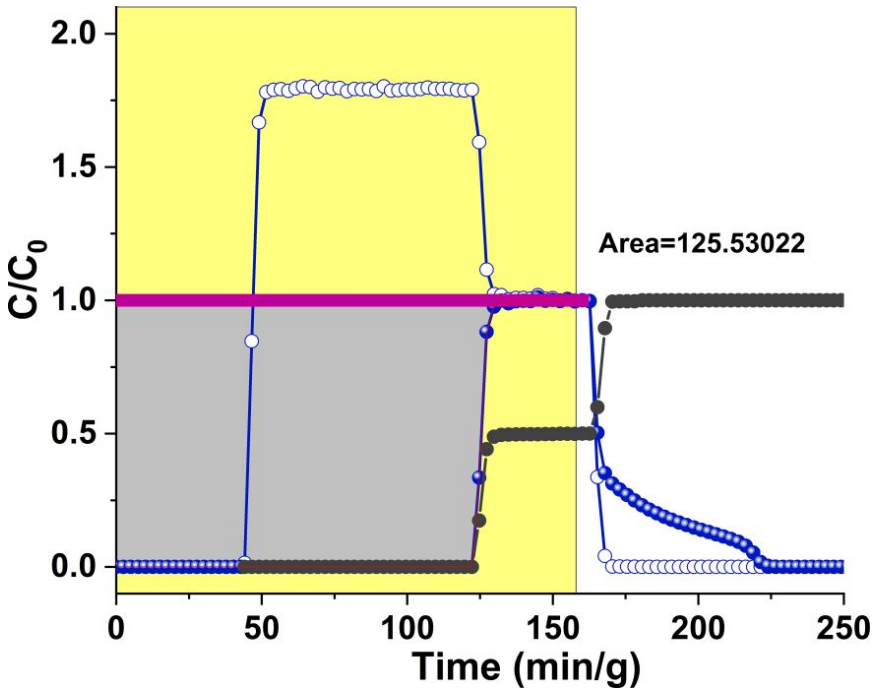

Figure S20. The adsorption capacity of C_3H_6 during the breakthrough process with flow rate of 1.7 $mL \cdot min^{-1}$ at 318 K.

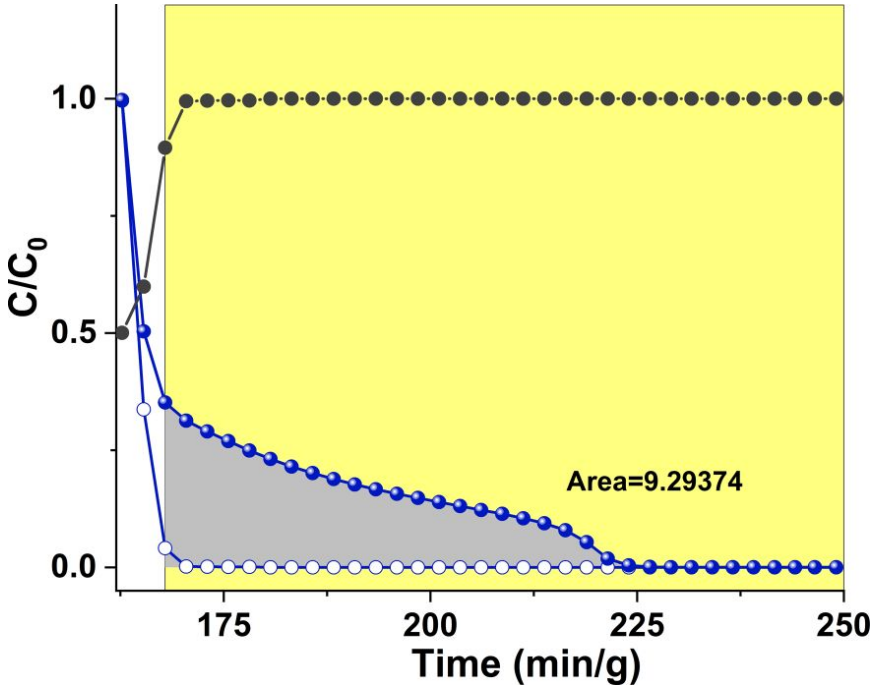

Figure S21. The C_3H_6 recovery of 3.6 $mol \cdot kg^{-1}$ with purity ≥99.5% during desorption process with flow rate of 1.7 $mL \cdot min^{-1}$ at 318 K.

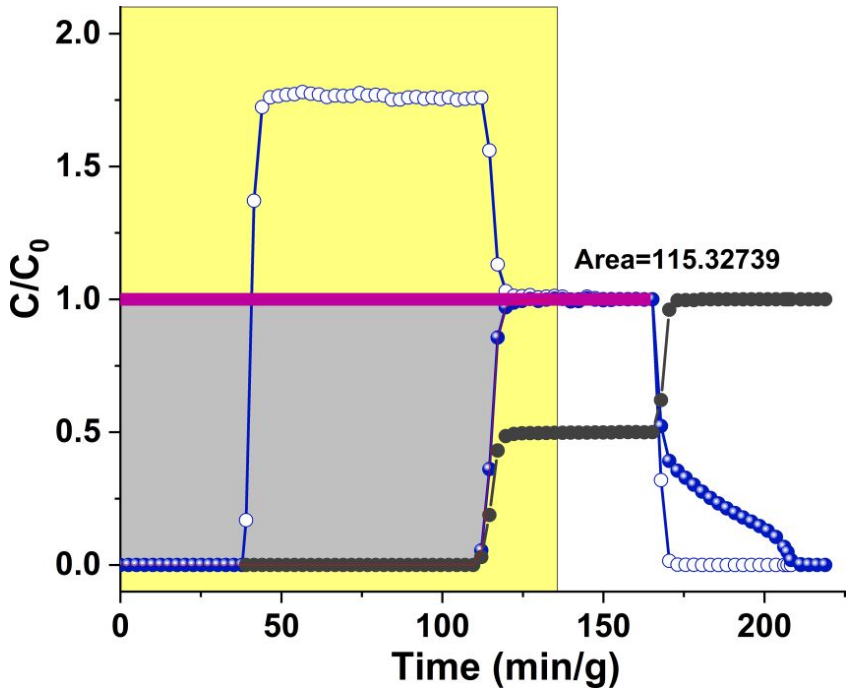

Figure S22. The adsorption capacity of C_3H_6 during the breakthrough process with flow rate of 1.7 mL·min^{-1} at 328 K.

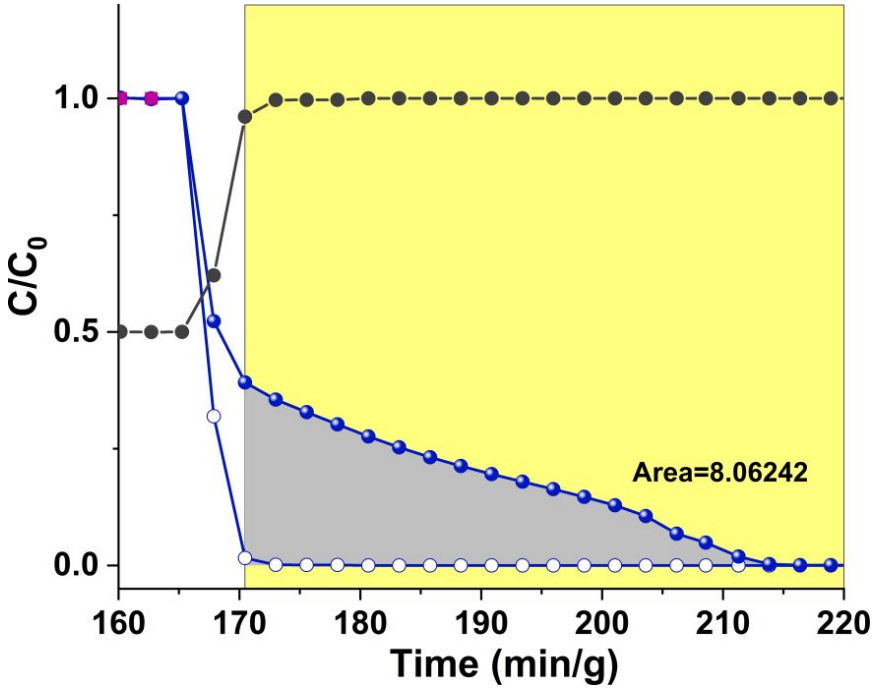

Figure S23. The C_3H_6 recovery of 3.1 mol·kg^{-1} with purity ≥99.5% during desorption process with flow rate of 1.7 mL·min^{-1} at 328 K.

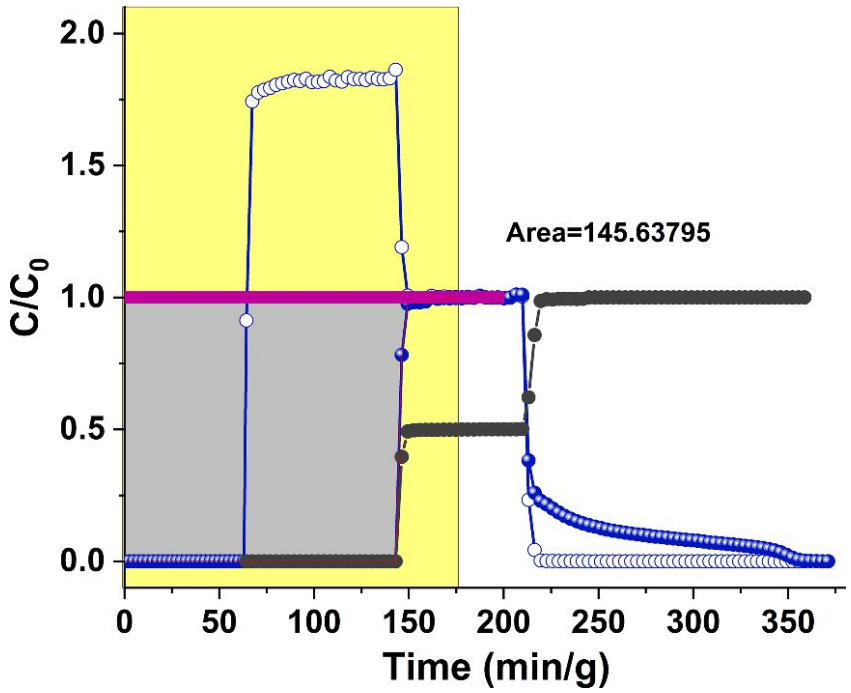

Figure S24. The adsorption capacity of C_3H_6 during the breakthrough process with flow rate of 1.7 mL·min^{-1} under 33% RH atmosphere.

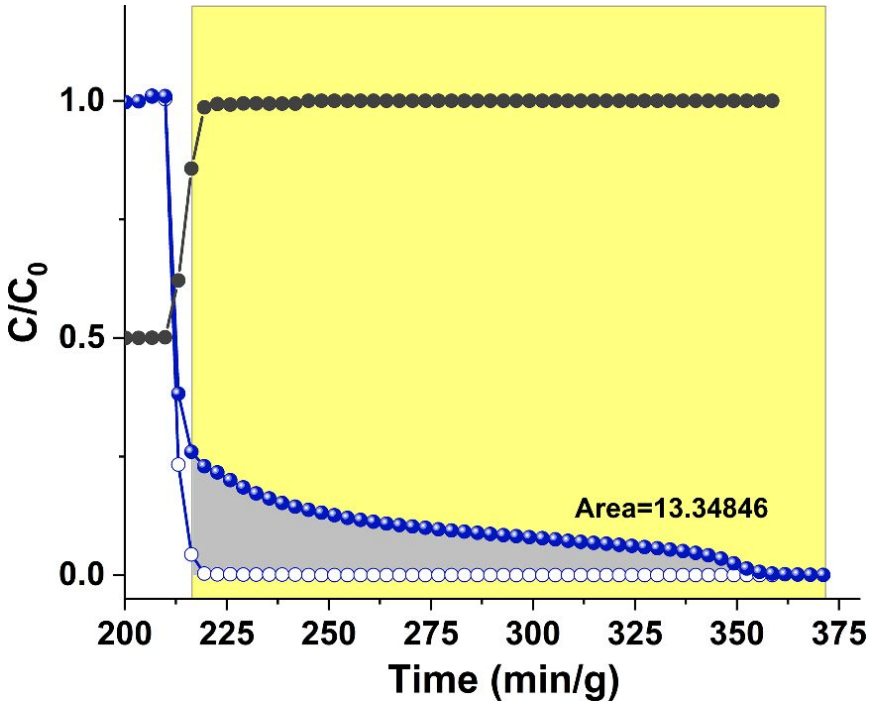

Figure S25. The C_3H_6 recovery of 4.4 mol·kg^{-1} with purity ≥99.5% during desorption process with flow rate of 1.7 mL·min^{-1} under 33% RH atmosphere.

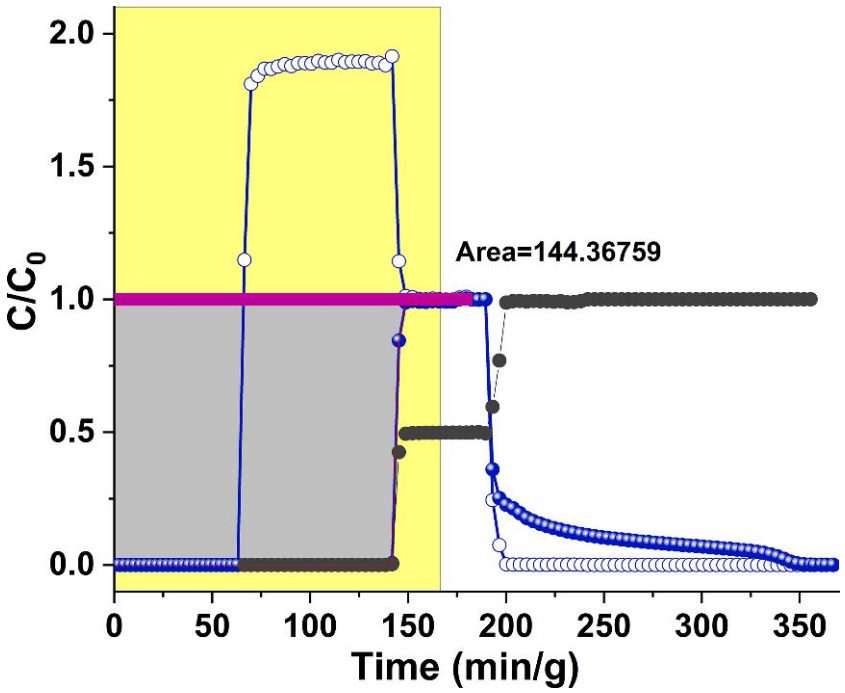

Figure S26. The adsorption capacity of C_3H_6 during the breakthrough process with flow rate of 1.7 mL·min^{-1} under 75% RH atmosphere.

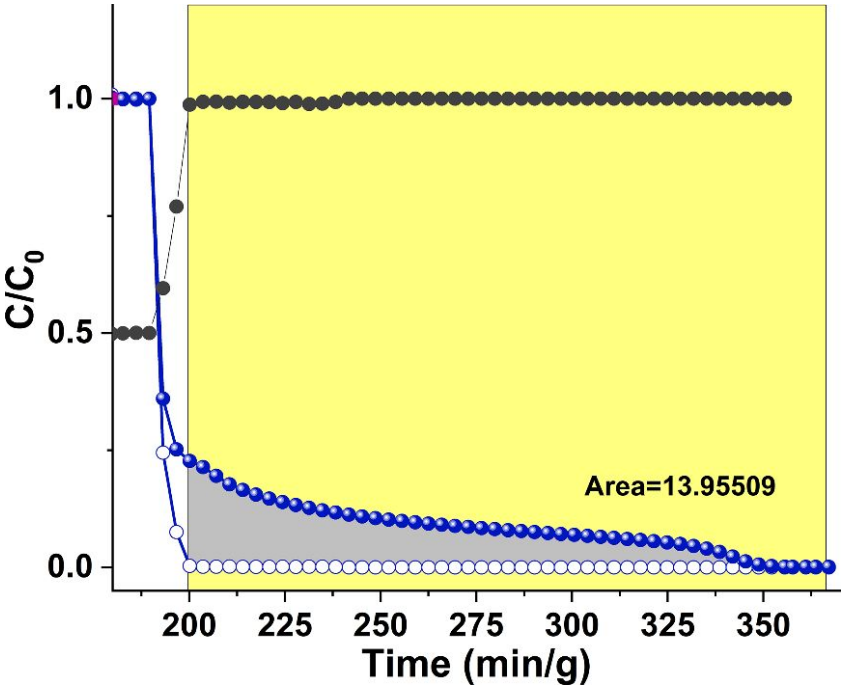

Figure S27. The C_3H_6 recovery of 4.4 mol·kg^{-1} with purity ≥99.5% during desorption process with flow rate of 5.0 mL·min^{-1} under 75% RH atmosphere.

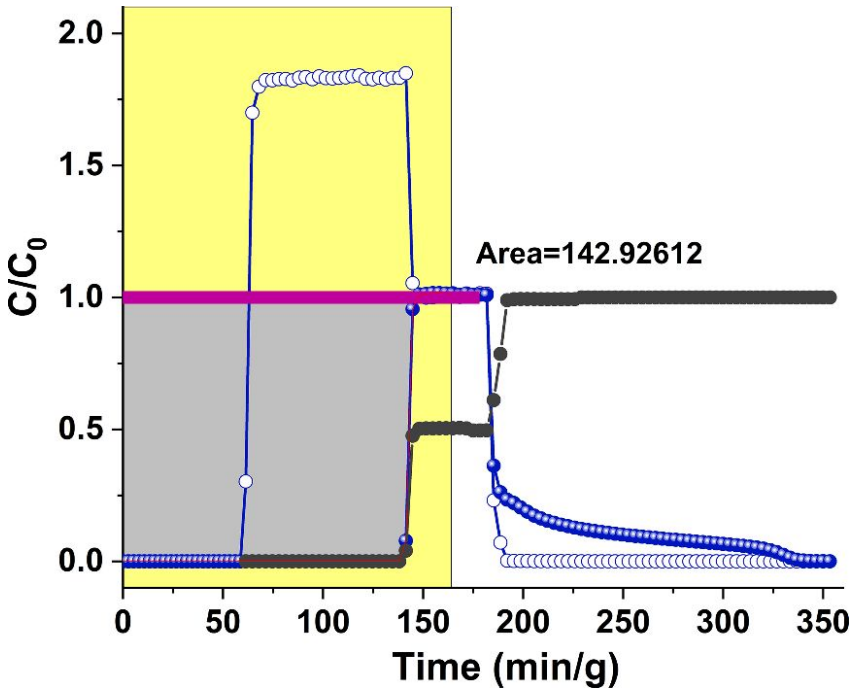

Figure S28. The adsorption capacity of C_3H_6 during the breakthrough process with flow rate of 1.7 mL·min^{-1} under 100% RH atmosphere.

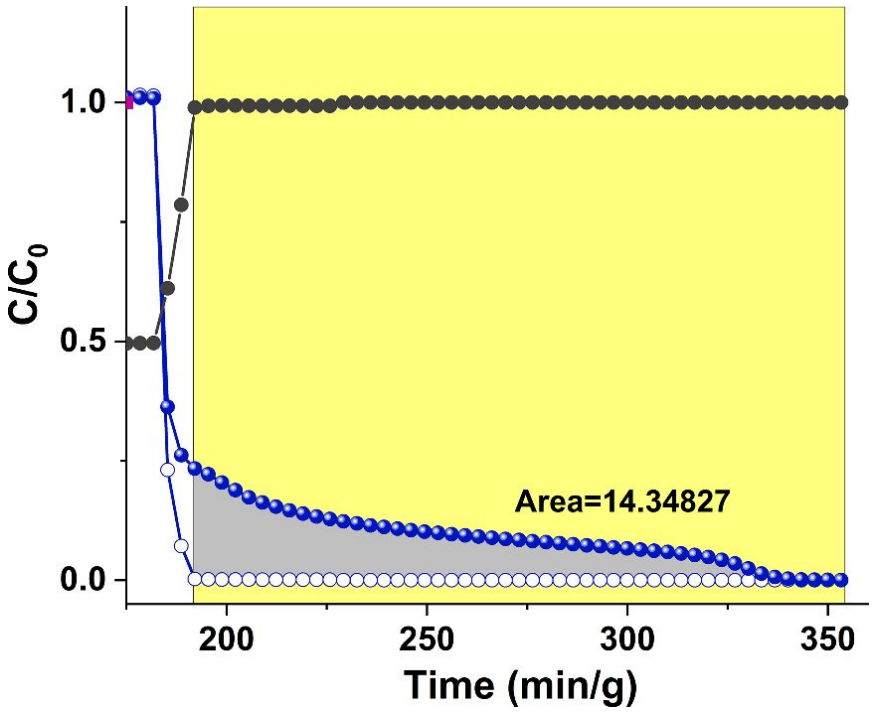

Figure S29. The C_3H_6 recovery of 4.3 mol·kg^{-1} with purity ≥99.5% during desorption process with flow rate of 1.7 mL·min^{-1} under 100% RH atmosphere.

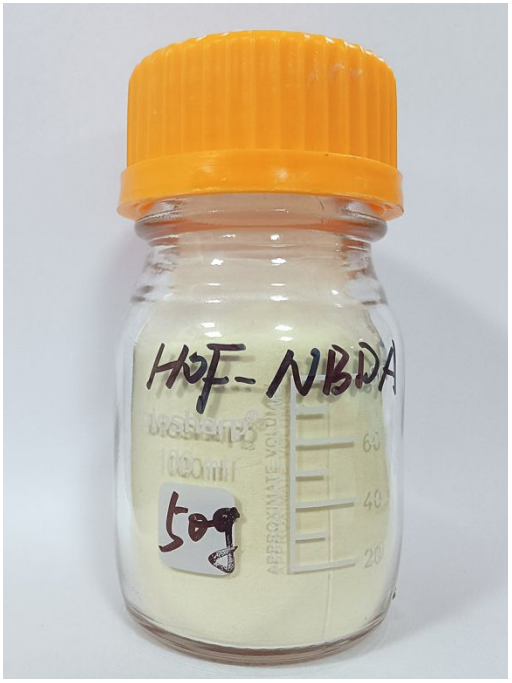

Figure S30. The photograph of the scale-up synthesized HOF-NBDA crystals.

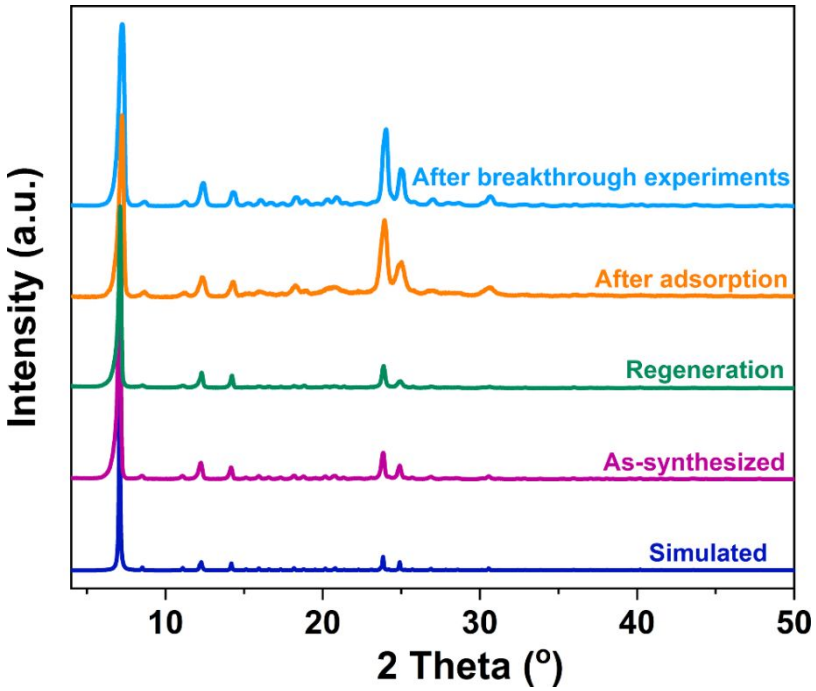

Figure S31. The Power X-ray diffraction (PXRD) patterns of HOF-NBDA.

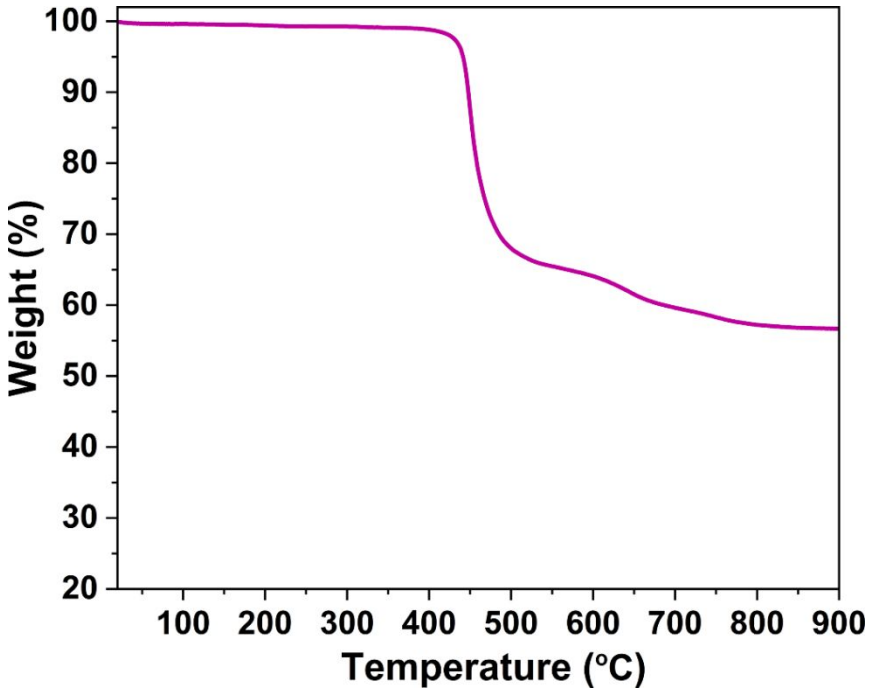

Figure S32. TGA curve of HOF-NBDA under nitrogen atmosphere.

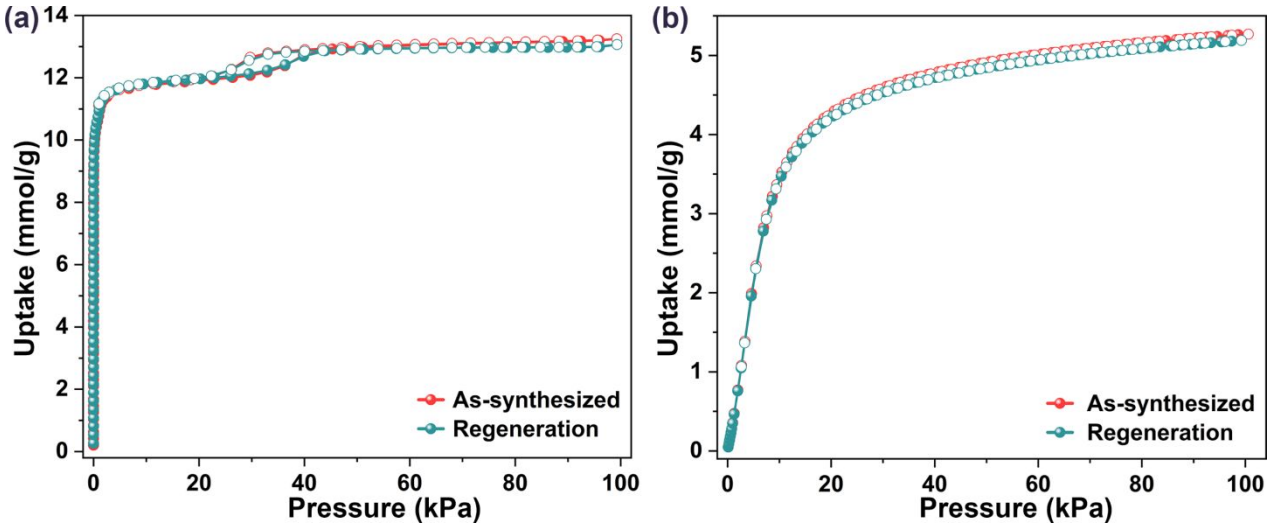

Figure S33. (a) N_2 (77 K) and (b) C_3H_6 (298 K) adsorption isotherms of as-synthesized HOF-NBDA and the regenerated HOF-NBDA.

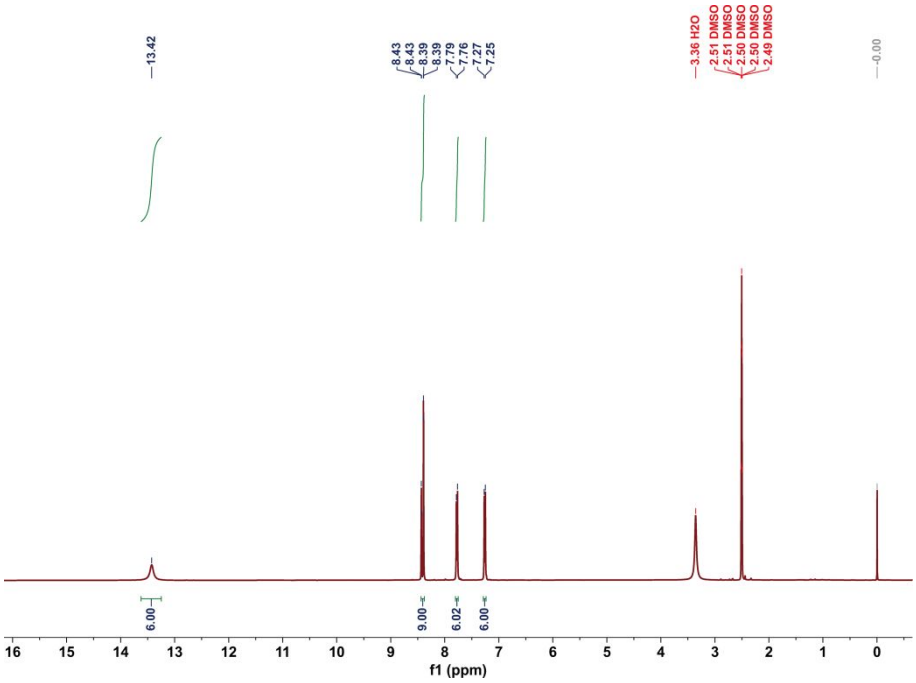

Figure S34. ^{1}H NMR spectrum of HOF-NBDA.

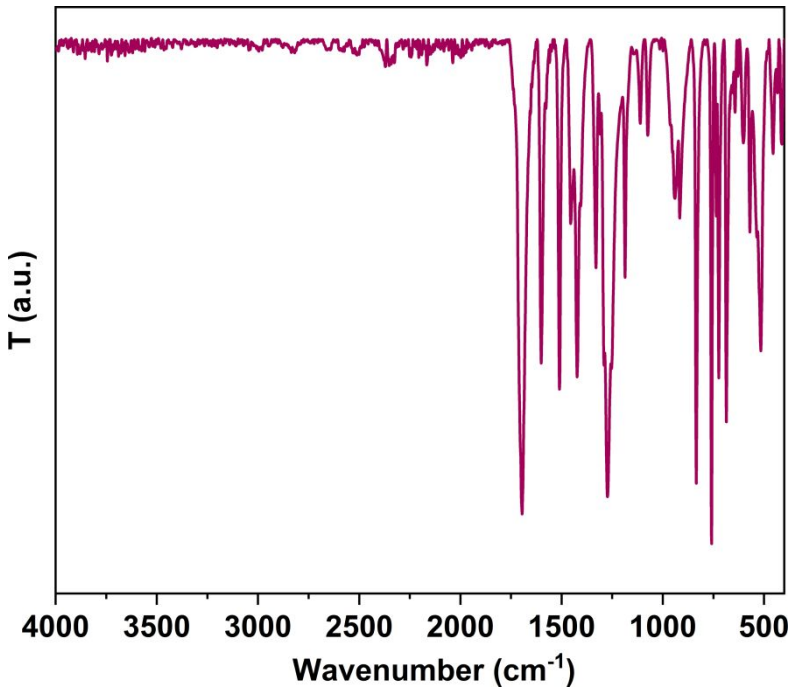

Figure S35. FT-IR spectrum of HOF-NBDA.

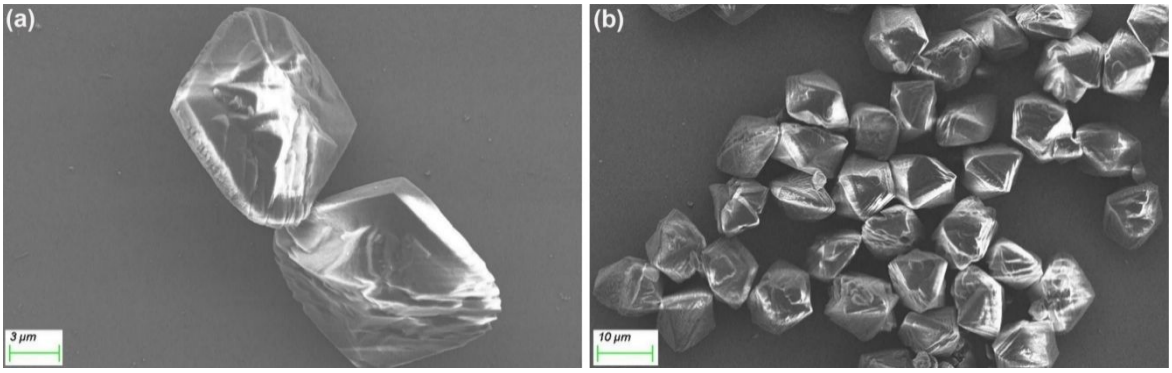

Figure S36. SEM images of HOF-NBDA.

Table S1. Summary of adsorption capacities and Q_{st} values of C_3H_6 and C_2H_4 respectively as well as C_2H_4/C_3H_6 (50/50, v/v) selectivity for different MOFs at 298 K under 100 kPa.

Adsorbents	**IAST**	**$Q_{st}(C_2H_4)$ (kJ·mol^{-1})**	**$Q_{st}(C_3H_6)$ (kJ·mol^{-1})**	**C_2H_4 uptake (mmol·g^{-1})**	**C_3H_6 uptake (mmol·g^{-1})**		**Ref.**
				100 kPa	**10 kPa**	**100 kPa**	
HOF-NBDA	**11.1**	**18.8**	**25.7**	**2.9**	**3.6**	**5.3**	**This work**
Mn-dtzip	8.6	24.6	35.1	3.4	3.1*	9.6	[8]
Zn-BPZ-SA	4.8	23.1	33.6	2.8	2.1	3.0	[9]
Zn-BPZ-TATB	7.4	18.3	28.1	4.1	3.5*	5.1	[10]
spe-MOF	7.7	22.5	29.6	2.2	1.3	10.5	[9,11]
$Zn_2(oba)_2(dmimpym)$	15.6	25.8	33.3	2.2	2.4	3.4	[12]
C-600	10.6	21.0	23.0	2.0*	1.4*	4.0*	[13]
UPC-33	5.7	10.3	48.9	1.4	1.1	4.2	[9,14]
NEM-7-Cu	8.6	22.5	36.9	1.3	1.1	3.4	[9,15]
iso-MOF-4	7.7	25.4	30.9	3.3	2.2	11.4	[16]

*These values are estimated from the adsorption isotherms reported before.

Table S2. The comparison of C_2H_4 (≥99.95%) and C_3H_6 (≥99.5%) productivities for C_2H_4/C_3H_6 (50/50,v/v) mixture.

Adsorbents	Separation Temperature	Productivity of C_2H_4 (≥99.95%)	Productivity of C_3H_6 (≥99.5%)	Ref.
HOF-NBDA	**298 K**	**5.7 mol·kg^{-1}**	**4.5 mol·kg^{-1}**	**This work**
Mn-dtzip	273 K	1.4 mol·kg^{-1}	-	[8]
	298 K	1.2 mol·kg^{-1}	-	
Zn-BPZ-SA	273 K	1.8 mol·kg^{-1}	-	[9]
	298 K	1.0 mol·kg^{-1}	-	
Zn-BPZ-TATB	273 K	4.8 mol·kg^{-1}	3.5 mol·kg^{-1}	[10]
	298 K	4.5 mol·kg^{-1}	2.7 mol·kg^{-1}	
spe-MOF	298 K	3.0 mol·kg^{-1}	-	[11]
$Zn_2(oba)_2(dmimpym)$	273 K	2.2 mol·kg^{-1}	-	[12]
	298 K	1.6 mol·kg^{-1}	-	

Table S3. The C_2H_4 (≥99.95%) and C_3H_6 (≥99.5%) productivities for HOF-NBDA at different flow rates.

Flow rate	Productivity of C_2H_4 (≥99.95%)	Productivity of C_3H_6 (≥99.5%)
1.7 mL·min^{-1}	5.7 mol·kg^{-1}	4.5 mol·kg^{-1}
	127.34 L·kg^{-1}	100.64 L·kg^{-1}
2.5 mL·min^{-1}	5.6 mol·kg^{-1}	4.5 mol·kg^{-1}
	125.49 L·kg^{-1}	100.30 L·kg^{-1}
3.4 mL·min^{-1}	5.6 mol·kg^{-1}	4.5 mol·kg^{-1}
	125.24 L·kg^{-1}	100.90 L·kg^{-1}
4.2 mL·min^{-1}	5.6 mol·kg^{-1}	4.5 mol·kg^{-1}
	124.32 L·kg^{-1}	100.37 L·kg^{-1}
5.0 mL·min^{-1}	5.5 mol·kg^{-1}	4.4 mol·kg^{-1}
	124.13 L·kg^{-1}	99.33 L·kg^{-1}

Table S4. The C_2H_4 (≥99.95%) and C_3H_6 (≥99.5%) productivities for HOF-NBDA at different temperatures.

Separation temperature	Productivity of C_2H_4 (≥99.95%)	Productivity of C_3H_6 (≥99.5%)
298 K	5.7 mol·kg^{-1}	4.5 mol·kg^{-1}
	127.34 L·kg^{-1}	100.64 L·kg^{-1}
303 K	5.2 mol·kg^{-1}	4.3 mol·kg^{-1}
	117.09 L·kg^{-1}	96.47 L·kg^{-1}
308 K	5.1 mol·kg^{-1}	4.1 mol·kg^{-1}
	114.83 L·kg^{-1}	92.17 L·kg^{-1}
318 K	5.0 mol·kg^{-1}	3.6 mol·kg^{-1}
	112.45 L·kg^{-1}	80.16 L·kg^{-1}
328 K	4.6 mol·kg^{-1}	3.1 mol·kg^{-1}
	102.92 L·kg^{-1}	70.26 L·kg^{-1}

Table S5. The C_2H_4 (≥99.95%) and C_3H_6 (≥99.5%) productivities for HOF-NBDA under different humidity.

Separation humidity	Productivity of C_2H_4 (≥99.95%)	Productivity of C_3H_6 (≥99.5%)
0%	5.7 mol·kg^{-1}	4.5 mol·kg^{-1}
	127.34 L·kg^{-1}	100.64 L·kg^{-1}
33%	5.4 mol·kg^{-1}	4.4 mol·kg^{-1}
	119.91 L·kg^{-1}	98.31 L·kg^{-1}
75%	5.3 mol·kg^{-1}	4.4 mol·kg^{-1}
	117.86 L·kg^{-1}	97.69 L·kg^{-1}
100%	5.2 mol·kg^{-1}	4.3 mol·kg^{-1}
	115.43 L·kg^{-1}	97.24 L·kg^{-1}

Refs.

1. Zhou Y, Chen C, Krishna R, Ji Z, Yuan D, Wu M. Tuning Pore Polarization to Boost Ethane/Ethylene Separation Performance in Hydrogen-Bonded Organic Frameworks. *Angew. Chem. Int. Ed.* **2023**, 62, e202305041.

2. Krishna R. The Maxwell-Stefan Description of Mixture Diffusion in Nanoporous Crystalline Materials. *Micropor. Mesopor. Mat.* **2014**, 185, 30-50.

3. Krishna R. Methodologies for Evaluation of Metal-Organic Frameworks in Separation Applications. *RSC Adv.* **2015**, 5, 52269-52295.

4. Krishna R. Screening Metal-Organic Frameworks for Mixture Separations in Fixed-Bed Adsorbers using a Combined Selectivity/Capacity Metric. *RSC Adv.* **2017**, 7, 35724-35737.

5. Krishna R. Methodologies for Screening and Selection of Crystalline Microporous Materials in Mixture Separations. *Sep. Purif. Technol.* **2018**, 194, 281-300.

6. Krishna R. Metrics for Evaluation and Screening of Metal-Organic Frameworks for Applications in Mixture Separations. *Acs Omega.* **2020**, 5, 16987-17004.

7. Krishna R. Synergistic and Antisynergistic Intracrystalline Diffusional Influences on Mixture Separations in Fixed-Bed Adsorbers. *Precis. Chem.* **2023**, 1, 83-93.

8. Zhang L, Ma L-N, Wang G-D, Hou L, Zhu Z, Wang Y-Y. A New Honeycomb MOF for C_2H_4 Purification and C_3H_6 Enrichment by Separating Methanol to Olefin Products. *J. Mater. Chem. A* **2023**, 11, 2343–2348.

9. Wang G-D, Krishna R, Li Y-Z, Ma Y-Y, Hou L, Wang Y-Y, Zhu Z. Rational Construction of Ultrahigh Thermal Stable MOF for Efficient Separation of MTO Products and Natural Gas. *ACS Materials Lett.* **2023**, 5, 1091–1099.

10. Wang G-D, Li Y-Z, Shi W-J, Hou L, Wang Y-Y, Zhu Z. Active Sites Decorated Nonpolar Pore-Based MOF for One-step Acquisition of C_2H_4 and Recovery of C_3H_6. *Angew. Chem. Int. Ed.* **2023**, 62, e202311654.

11. Fang H, Zheng B, Zhang ZH, Li HX, Xue DX, Bai J. Ligand-Conformer-Induced Formation of Zirconium-Organic Framework for Methane Storage and MTO Product Separation. *Angew. Chem. Int. Ed.* **2021**, 60, 16521–16528.

12. Li Y-Z, Wang G-D, Krishna R, Yin Q, Zhao D, Qi J, Sui Y, Hou L. A Separation MOF with O/N Active Sites in Nonpolar Pore for One-step C_2H_4 Purification from C_2H_6 or C_3H_6 Mixtures. *Chem. Eng. J.* **2023**, 466, 143056.

13. Lyu H, Zhu J, Zhou B, Cao H, Duan J, Chen L, Jin W, Xu Q. Structure-Directed Fabrication of Ultrathin Carbon Nanosheets from Layered Metal Salts: A Separation and Supercapacitor Study. *Carbon* **2018**, 139, 740-749.

14. Fan W, Wang Y, Zhang Q, Kirchon A, Xiao Z, Zhang L, Dai F, Wang R, Sun D. An Amino-Functionalized Metal-Organic Framework, Based on a Rare $Ba_{12}(COO)_{18}(NO_3)_2$ Cluster, for Efficient $C_3/C_2/C_1$ Separation and Preferential Catalytic Performance. *Chem. Eur. J.* **2018**, 24, 2137-2143.

15. Liu X, Hao C, Li J, Wang Y, Hou Y, Li X, Zhao L, Zhu H, Guo W. An Anionic Metal–Organic Framework: Metathesis of Zinc(II) with Copper(II) for Efficient C3/C2 Hydrocarbon and Organic Dye Separation. *Inorg. Chem. Front.* **2018**, 5, 2898–2905.

16. Fan W, Wang X, Zhang X, Liu X, Wang Y, Kang Z, Dai F, Xu B, Wang R, Sun D. Fine-Tuning the Pore Environment of the Microporous Cu-MOF for High Propylene Storage and Efficient Separation of Light Hydrocarbons. *ACS Cent. Sci.* **2019**, 5, 1261–1268.